Anti-Cancer Agents in Medicinal Chemistry, 2025, *25*, 499-516

RESEARCH ARTICLE

In vivo, *In vitro*, and *In silico* Studies of Umbelliferone and Irinotecan on MDA-MB-231 Breast Cancer Cell Line and *Drosophila melanogaster* Larvae

Erkut Tamtürk[1,*], Serap Yalçın[2], Fahriye Ercan[3] and Aydın Süzü Tuncbilek[1]

[1]*Department of Biology, Faculty of Art and Sciences, Erciyes University, 38100, Kayseri, Türkiye;* [2]*Department of Medical Pharmacology, Faculty of Medicine, Kırşehir Ahi Evran University, 40100, Kırşehir, Türkiye;* [3]*Department of Plant Protection, Faculty of Agriculture, Kırşehir Ahi Evran University, 40100, Kırşehir, Türkiye*

Abstract: ***Aims*:** Deaths from cancer are still very common all over the world and continue to be the focus of scientific research. Chemotherapy is one of the primary treatments used to prevent deaths from cancer. Side effects of chemotherapeutic drugs and resistance of cells to drugs are essential problems that limit the treatment process. Drug combination therapy is regarded as a significant application that inhibits the growth of tumors and is anticipated to provide a solution for the issues encountered. The combination therapy aims at a synergistic effect that will limit drug resistance and cytotoxic effects with appropriate drug combinations. In this context, we aim to investigate the *in vitro*, *in vivo,* and *in silico* effects of single and combined doses of umbelliferone and irinotecan, known for their anticarcinogenic and curative effects, on MDA-MB-231 breast cancer cell lines and the model organism *Drosophila melanogaster*.

***Background*:** Irinotecan is currently used as an anticarcinogenic drug. Anticarcinogenic effects of umbelliferone have also been detected. The *in vivo, in vitro,* and *in silico* impacts of single and combined doses use of these two agents are not yet available in the literature.

***Objective*:** This study aims to determine the anticarcinogenic effects of single and combined use of umbelliferone and irinotecan at the molecular level. It also attempts to determine the binding energies of chemicals to cancer-related proteins through docking and molecular dynamic studies.

***Methods*:** The cytotoxic effects of individual and combinational doses of umbelliferone and irinotecan on the MDA-MB-231 cell line and *D. melanogaster* were calculated by XTT and probit analyses. IC_{50} values for the cancer cells, LC_{50}, and LC_{99} values for *D. melanogaster* were found. Gene expression analysis was performed to determine the effects of chemical agents on miR-7, miR-11, and miR-14, and their expression levels were found. The sequences of miRNAs not found in the literature were determined, and their molecular imaging was performed. In addition, the binding energies of irinotecan and umbelliferone to Bcl-2, Bad, and Akt1 proteins, which are known to have apoptotic effects, were found by the molecular docking method. Molecular dynamics studies of Bad proteins and chemicals were also performed. The drug potential of chemicals was determined by ADME/T analysis.

***Results*:** The cytotoxic effect on cells was calculated, and the IC_{50} value of umbelliferone was calculated as 158 µM, the IC_{50} value of irinotecan was calculated as 48,3 µM and the IC_{50} value was calculated as 20 µM. In the probit analysis performed to calculate the cytotoxic effects of drugs on *D. melanogaster,* the LC_{50} value of umbelliferone was 2,5 µM, and the LC_{99} value was 13,4 µM. The LC_{50} value of irinotecan was found to be 0,1 µM, and the LC_{99} value was 0,28 µM. It was concluded that single and combined doses of chemicals in the invasion experiment significantly affected the spread of cells. As a result of expression analysis, a significant increase in Hsa-miR-7 (*Homo sapiens* miRNA-7*)*, Hsa-miR-14 (*Homo sapiens* miRNA-14*),* and Hsa-miR-11(*Homo sapiens* miRNA-11*)* expression was observed in cells treated with umbelliferone irinotecan compared to the control groups.

***Conclusion*:** In our study, it can be concluded that the cytotoxic effects of individual and combination doses of umbelliferone and irinotecan on MDA-MB-231 cells and *D. melanogaster* larvae are significant. In addition, the effects of umbelliferone and irinotecan on the expression level of miR-7, which is a common *D. melanogaster* and human miRNA, should be widely investigated. Expression analyses and docking studies of Hsa-miR-11 and Hsa-miR-14, which have been newly studied and are not in data repositories, are important for cancer research. In particular, the expression and binding energy of these miRNAs in new drug combinations and the expression level in different cancer cell lines are important for future studies. Another crucial point is that *in vivo* tests using different model species validate the usage of drugs at both single and mixed dosages.

***Other*:** As a result of this study, the *in vivo, in vitro,* and *in silico* effects of single and combined doses of umbelliferone and irinotecan were determined. In future studies, it would be useful to determine the binding energies of umbelliferone and irinotecan to other cancer-related proteins and to find their interactions with different miRNAs. Additionally, studies on different model organisms are also important.

Keywords: Umbelliferone, Irinotecan, breast cancer, *Drosophila melanogaster*, *in silico* analyses, miRNA.

ARTICLE HISTORY

Received: July 02, 2024
Revised: September 20, 2024
Accepted: September 24, 2024

DOI:
10.2174/0118715206340868241018075528

*Address correspondence to this author at the Department of Biology, Faculty of Art and Sciences, Erciyes University, 38100, Kayseri, Türkiye; E-mail: erkuttamturk@gmail.com

1875-5992/25 $65.00+.00

1. INTRODUCTION

Cancer is one of the most important diseases in the world, and studies for new treatments continue. The cell cultures and animal experiments have been used in new drug development studies. *D. melanogaster* is used as a model organism in many fields, especially in molecular biology [1]. Research conducted on *D. melanogaster* offers valuable insights into signal transmission networks, tumor-forming genes, and potentially evolutionarily protected apoptotic or anti-apoptotic genes. These insights are applicable to studies on cancer as well as many other disorders. First identified in *Drosophila*, signal transduction pathways, including EGFR/RTK-Ras, PI3K, Notch, Wnt, Jak-STAT, Hedhegog, and TGF-β are believed to be evolutionarily conserved. The *Drosophila* tumor suppressor gene dPTEN (*Drosophila* PTEN) is the homolog of the mammalian tumor suppressor gene phosphatase and tensin homolog (PTEN) [2]. Numerous factors can contribute to the development of cancer. Therefore, doing research using a variety of techniques, including *in vivo*, *in vitro*, and *in silico*, may yield more accurate results.

In the vast majority of cancer diseases (95%), the effects of genetic and environmental factors have been encountered together. Although angiogenesis, inflammation, and altered cell metabolism are clues for carcinogenesis, both genetic and environmental factors are thought to be effective in these processes [3, 4].

The method used in cancer treatments, also known as the traditional treatment method, is chemotherapy. Chemotherapy was used in the 1940s. Before 1950, the fight against cancer was mostly done with surgical methods, but after 1960, chemotherapy began to be used much more [5]. The side effects of chemotherapy drugs are an important process that determines the outcome of the treatment. Another important situation is that cancer cells acquire drug resistance. It is known that one of the ways to minimize drug resistance is the simultaneous use of two different chemical agents with different effects and mechanisms. Combination chemotherapy aims to achieve synergy by using different chemicals together and to achieve therapeutic progress by discovering ideal drug partners [6]. In a study conducted on 1581 metastatic breast cancer patients, combination chemotherapy treatment using doxorubicin and an alkylating agent showed more positive results than classical chemotherapy. In this treatment, doxorubicin, fluorouracil, and cyclophosphamide (FAC) were used in the induction phase, and cyclophosphamide, methotrexate, and fluorouracil were used in the continuation of the treatment [6, 7].

Irinotecan (Camptosar®, CPT-11), which is known for its cytotoxic effects, was first approved for use in cancer treatments in Japan. It has been reported that the drug, which has been used for more than twenty years, makes a great contribution to cancer treatments [8]. In recent years, irinotecan has been used frequently in the treatment of pediatric sarcoma, rhabdomyosarcoma and Ewing sarcoma, neuroblastoma, nephroblastoma, neuroectodermal, and leiomyosarcoma diseases [9]. Important findings were found in a study examining irinotecan's impact on colon cancer. Irinotecan is known to extend the course of treatment [10]. Additionally, it has been determined that applying it in conjunction with medications like bevacizumab improves survival [10]. Umbelliferone is a 7-hydroxycoumarin derived from the Apiaceae family known for its antioxidant, anticarcinogenic, anti-inflammatory, antidiabetic, antimicrobial, and antibacterial properties [11, 12]. Umbelliferon, which is well-known for its anticarcinogenic effects, is also promising for future studies. In a study conducted on hepatocellular carcinoma cells, umbelliferone was found to induce apoptosis, arrest the cell cycle, and exert antitumor effects through DNA fragmentation [13]. The apoptotic action of umbelliferone has been elucidated in a study looking into its impact on prostate cancer [14]. *Aegle marmelos* (L.) Corr (*Rutaceae*) plant roots were used to isolate umbelliferone β-D-galactopyranoside, which was given to mice in a different investigation. According to Kumar *et al*. (2013) [15], the application led to the conclusion that umbelliferone β-D-galactopyranoside exhibits antihyperlipidemic, antioxidant, and antidiabetic properties. Albino mice were used in a different investigation on this topic. The experiment's results indicate that umbelliferone may have an anticarcinogenic effect on lung cancer [16]. Another study that looked into how umbelliferone affected MKN-45 and MIA-PaCa-2 cell lines also produced some significant findings in which cytotoxic properties of umbelliferone have been shown

In this study, the cytotoxic, molecular, *in vitro*, and *in silico* effects of umbelliferone and irinotecan on the MDA-MB-231 breast cancer cell line and the model organism *D. melanogaster* were investigated. In this research, IC_{50}, $LD_{50,}$ and LD_{99} values of irinotecan and umbelliferone were calculated on cells and model organisms. Additionally, the metastatic effects of irinotecan and umbelliferone were analyzed on MDA-MB-231 cell lines. To better determine the effects of irinotecan and umbelliferone at the molecular level, RNA was isolated from drug-treated and untreated MDA-MB-231 cell lines and D. melanogaster larvae. The expression levels of miR-7, miR-11, and miR-14 of the drugs were calculated. Docking studies were carried out to determine the binding energies of Bcl-2, Bad, and Akt-1 proteins, as well as umbelliferon and irinotecan. Molecular dynamics studies of Bad proteins and chemicals were performed.

This work aims to investigate the effects of two compounds, umbelliferone, and irinotecan, which are known to have anticarcinogenic effects, on *D. melanogaster* and MDA-MB-231 breast cancer cell lines *in vivo*, *in vitro*, and *in silico*. Furthermore, by examining the effects of single and combination chemical dosages on the expression levels of specific miRNAs, the goal was to ascertain the molecular effects of chemicals. Molecular modeling studies were utilized to visualize miRNAs and apoptotic proteins. The combined consideration of *in vivo*, *in vitro*, and *in silico* investigations led to an interpretation of the cytotoxic effects of substances in conjunction with docking studies.

2. MATERIALS AND METHODS

2.1. Chemical Structure of Umbelliferon and Irinotecan

The molecular weight of irinotecan, whose chemical formula is $C_{33}H_{38}N_4O_6$, is 586.7 g/mol. Irinotecan is a member of the pyranoindolizinoquinoin group [17]. Umbelliferon has a molecular weight of 162.14 g/mol. It is a natural product of the coumarin family [18], and can be distinguished from plant extracts using methanol [19]. The molecular formula of umbelliferone is $C_9H_6O_3$ [20]. Spectroscopic techniques isolated umbelliferone from the *Acacia nilotica* plant of the Mimosceae family, which is used for viral treatments (cold, flu), bacterial (diarrhea), dysentery, fungal, and leucoderma diseases, and shows antimutagenic and cytotoxic activities [21]. The 2- and 3-dimensional structures and formulas of umbelliferon and irinotecan are shown in Table **1**.

2.2. Cell Culture

In the study, MDA-MB-231 breast cancer cell lines in the Medical Pharmacology Laboratory of Kırşehir Ahi Evran University Faculty of Medicine were used. Cell lines were developed in 10% (v/v) fetal bovine serum (FBS), 1% gentamicin antibiotic, and 88% (v/v) RPMI-1640 medium in a 75 cm^2 flask. Cell lines were allowed to grow in a 5% CO_2, 37°C incubator. When the flask bottom was approximately 80% covered with cells, the trypsin-EDTA enzyme was used to remove the cells from the surface. The cell passage number is 15.

Table 1. The chemical properties of umbelliferone and irinotecan.

Chemical Agent	Formula	2D Structure	3D Structure	References
Umbelliferon	$C_9H_6O_3$	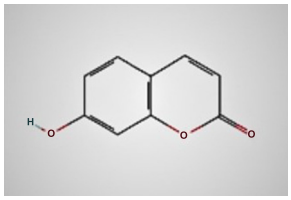	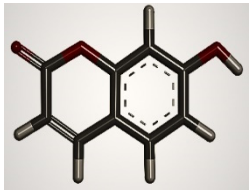	https://pubchem.ncbi.nlm.nih.gov/compound/5281426#section=3D-Conformer PubChem İd: 5281426
Irinotecan	$C_{33}H_{38}N_4O_6$	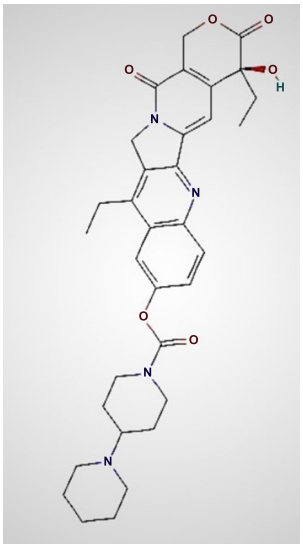	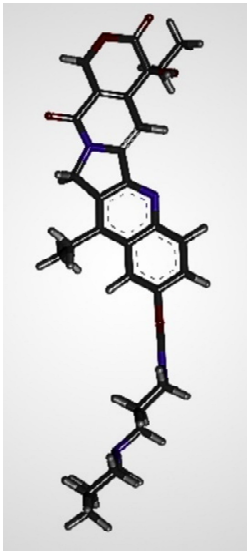	https://pubchem.ncbi.nlm.nih.gov/compound/Irinotecan. PubChem İd: 60838

2.3. Cytotoxicity Analyses on MDA-MB-231 and *D. melanogaster*

Cytotoxicity analysis was performed using probit analysis in *D. melanogaster* larvae and XTT analysis in MDA-MB-231 cell lines. MDA-MB-231 cell lines were seeded in 96-well plates. The first vertical row in the wells was considered medium control, and no chemicals were added. The second vertical row of cells was designated as control. Umbelliferon and irinotecan were added in serial dilutions starting from the third vertical row. Umbelliferon was applied in serial dilutions, increasing by 100 µM in each well. Irinotecan was applied in serial dilutions, increasing by 20 µM in each well. XTT reagent kit was added to the wells after 72 hours and kept in the incubator for 4 hours. The absorbance value on the plates was read on a spectrophotometer at 450 nm. As a result of the analyses, IC_{50} values were found for MDA-MB-231 cell lines as a result of the applications of each chemical separately and in combination. Various doses of chemicals were given to *D. melanogaster* larvae. The critical dose LC_{50}, which killed half of the larvae, and the critical dose LD_{99}, which killed almost all of the larvae, were found and recorded.

2.4. Wound-healing Assay

The wound-healing assay, an early and cost-effective technique, is straightforward and mimics *in vitro* directional cell migration, resembling the process of wound healing observed in living organisms [22]. In this analysis, MDA-MB-231 cell lines were added to 96-well plates. After 24 hours, a smooth line was drawn from the top to the bottom of each well. The IC_{50} doses of Umbelliferon (158 µM) and irinotecan (48.3 µM) were administered separately and together (20 µM) to different experimental wells. Photographs were taken at 0, 24, 48, and 72 hours.

2.5. Invasion Assay

Cell culture inserts were embedded within 24-well plates, and 100 µL of diluted matrigel at a 1:10 ratio was introduced after 48 hours; the desired matrigel structure was established, RPMI-1640 medium supplemented with fetal bovine serum (FBS) was added into the wells. After a 48-hour incubation period, the cells were immobilized by exposure to 4% formaldehyde for 15 minutes at room temperature, and they were subsequently dyed with a 10% Giemsa stain for 20 minutes [23].

2.6. *In vivo* Analyses

The model organism D. melanogaster was used in the experiment to perform *in vivo* analyses. *D. melanogaster* cultures were grown in falcon tubes with a medium at 25°C and approximately 60% relative humidity. *D. melanogaster* media were prepared using 50 g corn flour, 50 g granulated sugar, 35 g brewer's yeast, 10 g agar, 1000 ml distilled water, and 5ml propionic acid [24]. Larvae that reached the third instar stage were placed in petri dishes, with 50 larvae in each dish. Umbelliferon and irinotecan were then applied to the larvae at varying doses. In the study conducted to calculate the cytotoxic effect of umbelliferone and irinotecan on *D. melanogaster* larvae, firstly 250, 500, 1000, and 6000 µM umbelliferon were applied to the larvae. After 24 hours, surviving and dead larvae were counted. Additionally, irinotecan was applied to 50 *D. melanogaster* larvae at doses of 25, 50, and 100 µM, and the surviving larvae were counted after 24 hours. At the end of 24 hours, live and dead larvae were counted. Probit analysis was performed based on the data obtained. As a result of the analyses, LC_{50} and LC_{99} values were calculated. Additionally, the effect of combined LC_{50} doses of chemicals on larvae was calculated as percent mortality.

2.7. cDNA Synthesis and RNA Isolation

IC_{50} values of umbelliferone and irinotecan were administered to MDA-MB-231 cell lines separately and in combination. Gene analysis and RNA isolation were performed from the samples obtained. GeneAll® Hybrid-R™ RNA isolation kit was used for RNA isolation. Samples for gene analysis were sent to Atlas Biotechnology Laboratory Materials Industry and Trade LTD. Hsa-miR-7, Hsa-miR-11, and Hsa-miR-14 gene expressions were calculated in umbelliferon and irinotecan applications. All applications here were performed according to the manufacturer's protocol. After determining the purity and concentrations of the RNA, cDNA synthesis was performed using the GeneAll® HyperScript™ (cat. no: 601-005) first-strand synthesis kit. Following cDNA synthesis, RT-PCR reactions were performed.

2.8. *In silico* Analyses

2.8.1. Molecular Docking Analysis

Two- and three-dimensional structures of umbelliferon and irinotecan were taken from PubChem (https://pubchem.ncbi.nlm.nih.gov/). Sequences of miRNAs were obtained from miRDB (http://www.mirdb.org/) and miRBase (https://mirbase.org/) [25]. Using these sequences, the two-dimensional structures of miRNAs were obtained from the Centroid Fold (http://rtools.cbrc.jp/centroidfold/) software site. Then, the three-dimensional structures of miRNAs were obtained from the RNA composer (https://rnacomposer.cs.put.poznan.pl/) [26] site. Autodock vina (https://vina.scripps.edu/) (Trott *et al*. 2010) [27] and MGL tools (https://ccsb.scripps.edu/mgltools/) programs were used as molecular docking programs. Bcl-2, Akt1, and Bad proteins were selected for Molecular Docking. In addition, the binding energies of umbelliferone and irinotecan to miR-7, miR-11, and miR-14 were calculated using the same program. The binding of ligands and proteins was visualized in three dimensions using the Pymol (https://pymol.org/2/) [28] program. Swissdock (http://www. swissdock.ch/) [29], a docking software program available over the internet, and Seamdock (https://bioserv.rpbs.univ-paris-diderot.fr/services/SeamDock/) [30] are used to confirm the docking work program was used.

2.8.2. ADME/T Analyses

ADME/T analysis was performed to reveal whether umbelliferone has drug properties. In this context, PDB files of the molecules were uploaded to the SwissADME program (http://www.swissadme.ch/index.php) [31] and radar graphs were shown.

2.8.3. miRNA Analyses

RNA was isolated from MDA-MB-231 breast cancer cell lines using the GeneAll® Hybrid-R™ RNA isolation kit, and human miR-7, miR-11, and miR-14 gene expression analyses were performed. RNA isolation was performed according to the protocols in this kit. Atlas Biotechnology Trading and Limited company performed expression analyses. Since Hsa-miR-11 and Hsa-miR-14 are miRNAs that have recently entered the literature, their sequences were taken from Atlas Biotechnology Trading and Limited company, and three-dimensional imaging and docking studies were performed according to these sequences. miR-11 (NCBI Series: GSE178917) (https://www.ncbi.nlm.nih.gov/geo/query/acc.cgi?acc=GSM5400833) and miR-14 (NCBI Series: GSE178917) (https://www.ncbi.nlm.nih.gov/geo/query/acc.cgi?acc=GSM5400836) are available in the National Library of Medicine data set.

The association of miR-7 with cancer and its presence in *D. melanogaster* was effective in selecting this miRNA in the study. Since Hsa-miR-11 and Hsa-miR-14 are new miRNAs that have entered the literature, no studies have been found yet, especially in the field of cancer. For this reason, these RNAs were chosen to investigate.

2.8.4. Molecular Dynamic Analyses

WebGro online application was chosen for molecular dynamics studies of proteins and ligand-protein complexes. The stabilities of the single and ligand-bound states of the proteins are shown graphically at 50 nc (nanosecond) simulation time [32-37].

3. RESULTS

3.1. Cytotoxicity Analyses

Umbelliferon, irinotecan, and drug combination (irinotecan+umbelliferon) were administered to MDA-MB-231 cell lines at a dose of IC_{50}. The cytotoxic effect on cells was calculated, and the IC_{50} value of umbelliferone was calculated as 158 µM, the IC_{50} value of irinotecan was 48.3 µM, and the IC_{50} value of the drug combination was calculated as 20 µM. The IC50 values of umbelliferon and irinotecan are shown in. Fig. (**1**), and the IC_{50} values of the drug combinations are shown in Fig. (**2**).

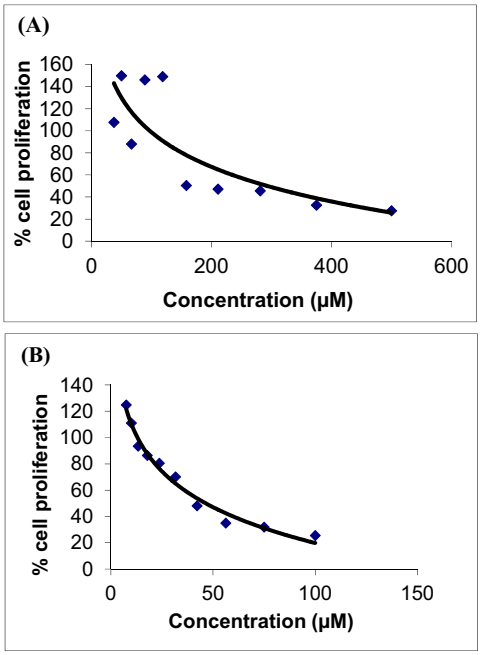

Fig. (1). (**A**) Figure showing cell proliferation rates as a result of umbelliferon application to MDA-MB-231 cell lines (**B**) Figure showing cell proliferation rates as a result of irinotecan application to MDA-MB-231 cell lines. (*A higher resolution / colour version of this figure is available in the electronic copy of the article*).

In the probit analysis performed to calculate the cytotoxic effects of drugs on *D. melanogaster*, the LC_{50} value of umbelliferone was found to be 2.5 µM, and the LC_{99} value was 13.4 µM. The LC_{50} value of irinotecan was 0.1 µM, and the LC_{99} value was 0.28 µM. LC_{50} and LC_{99} values of umbelliferon and irinotecan administered to *D. melanogaster* larvae are shown in Table **2**.

Since there has been no research on utilizing irinotecan and umbelliferon together, the combined dosage was calculated using LC_{50} values. These results were achieved by co-administering Irinotecan (0.1 µM) and Umbelliferon (2.5 µM). It was observed that 38% of the larvae died when the two drugs were applied together.

3.2. Wound-healing and Invasion Assay

Images of the control groups in the wound healing experiment at the end of 0 h, 24 h, and 48 h are shown in Fig. (**3**). At the end of 48 hours, it was observed that the opened channel remained wider in the groups administered umbelliferon, irinotecan, and drug com-

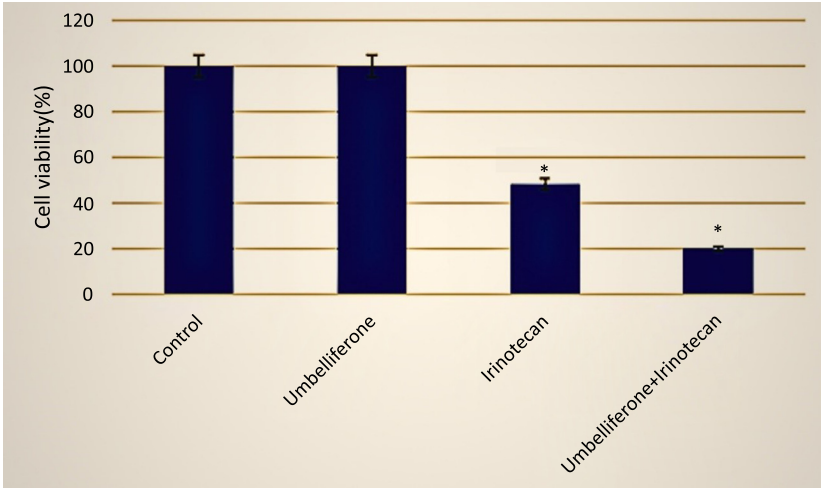

Fig. (2). Comparison of cell proliferation rates as a result of co-administration of umbelliferon and irinotecan to MDA-MB-231 cell lines with single dose applications. (*A higher resolution / colour version of this figure is available in the electronic copy of the article*).

binations compared to the control groups. The progress of MDA-MB-231 cells applied to umbelliferon, irinotecan, and drug combinations in the opened channel is shown in Fig. (**4**).

Table 2. LC_{50} and LC_{99} values of umbelliferon and irinotecan as a result of serial doses applied to *D. melanogaster* third instar larvae.

Duration (24 h)	N	LC_{50} µM	LC_{99} µM
Umbelliferon	50	2,5	13,4
Irinotecan	50	0,1	0,28

The narrowing occurring in the control groups in the wound healing experiment indicates the migration of cells under normal conditions. It was observed that this shrinkage was more limited in the cell lines treated with umbelliferon, irinotecan, and drug combination compared to the control groups.

The spread of MDA-MB-231 cell lines stained with 10% Giemsa dye prepared using invasion experiment protocols, without chemical application, was observed at 0, 24, and 48 hours, and the images were recorded as the control group. The invasions of MDA-MB-231 cell lines as a control group at 24, 48, and 72 hours are shown in Fig. (**5**). Invasion of cells was observed at the end of the 48th hour in the groups administered irinotecan, umbelliferon, and drug combination (umbelliferon and irinotecan), and the pictures were recorded in the experimental group. Invasion of MDA-MB-231 cells applied with umbelliferon, irinotecan, and drug combinations at the end of the 48th hour is shown in Fig. (**6**).

In the invasion experiment performed on cells stained with Giemsa dye, it is seen that the cells in the control groups initially showed an active spread. It is observed that this spread is limited in the groups administered by umbelliferon, irinotecan, and drug combinations. In the invasion experiment, the partial decrease in cells in the control group is due to excessive invasion of the cells. This decrease is clearly seen in the drug-administered groups.

3.3. Gene Expression Analysis

For gene expression analysis, RNA was isolated from cancer cells and *D.melanogaster* larvae, and then cDNA synthesis and gene expression levels were analyzed by RT-PCR. According to the analysis results, a statistically significant change was observed in miR-7, miR-11, and miR-14 expression levels when irinotecan was applied to cancer cell lines (Fig. **7**).

3.4. Two-dimensional Structures of miR-7, miR-11, and miR-14

Hsa-miR-7, Hsa-miR-11, and Hsa-miR-14 sequences were obtained as a result of receiving services from Atlas Biotechnology Laboratory Materials Industry and Trade LTD. The obtained miRNA sequences were converted into 2-dimensional miRNA structures using the Centroid Fold online software program. 3D images of miRNAs were prepared with Pymol and Discovery Studio 2021 programs. The sequence and 2D and 3D structure of Hsa-miR-7-5p are shown in Table **3**.

The sequence and 2D and 3D structure of Hsa-miR-11 are shown in Table **4**.

The sequence and 2D and 3D structure of Hsa-miR-14 are shown in Table **5**.

3.5. Molecular Docking

Bcl-2, Akt-1, Bad and BUFFY, CG15530, and Akt1 proteins, which are known to have apoptotic properties, were selected for molecular docking studies for humans and insects, respectively. Autodock Vina 1.5.6 program was used in docking studies, and the results were obtained from the online docking program Swissdock (http://www.swissdock.ch/) and Seamdock (https://bioserv.rpbs.univ-paris-diderot.fr/services/SeamDock). It was observed that the program used was compatible with the results of the online docking programs. PDB ID codes, Uniprot names, and 3D structures of Bcl-2, Akt-1, Bad and BUFFY, CG15530, and Akt1 proteins are shown in Table **6** [38].

The binding energy of BUFFY, CG15530, and Akt1 insect proteins, which are homologous to Bcl-2, BAD, and Akt1 proteins in *H. sapiens*, to umbelliferon and irinotecan ligands was also determined with Autodock Vina and Seamdock programs.

The Three-dimensional structures of *D. melanogaster* proteins were accessed from the UniProt protein data site [39]. The binding energies of umbelliferone and irinotecan to hsa-miR-7-5p, hsa-miR-11, and hsa-miR-14 are shown in Table **7**.

Binding energies of umbelliferone and irinotecan to Bcl-2 (1G5M), Akt1 (1H10), BAD (1G5J), BUFFY (AT16536p), dAkt1 (RAC serine/threonine-protein kinase), CG15530 (AT23209p) proteins are shown in Table **8**.

The binding energies of umbelliferon and irinotecan to *D. melanogaster* proteins were calculated using Autodock Vina, Swissdock, and Seamdock programs. The binding energies of

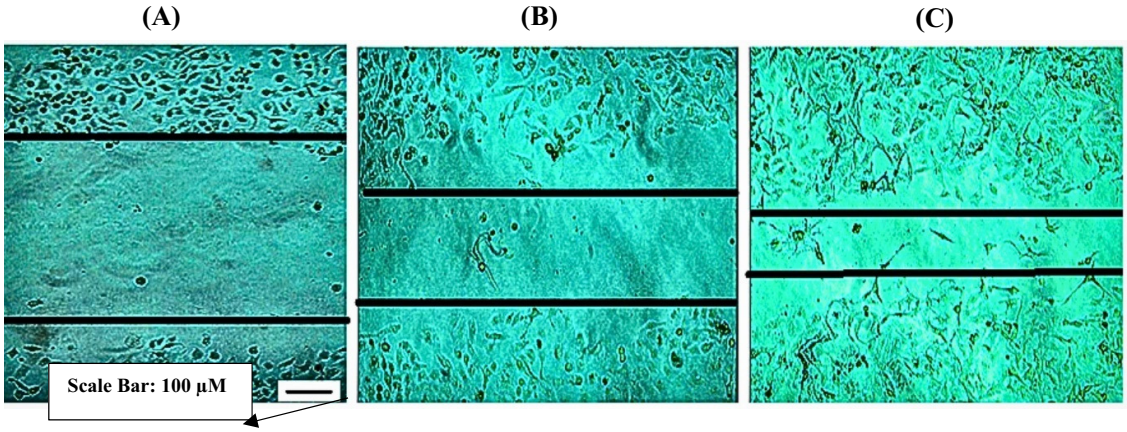

Fig. (3). MDA-MB-231 control 0 h (**A**): A wound was created in MDA-MB-231 breast cancer cells using a pipette tip and the image obtained under a light microscope was recorded. Control 24 h (**B**): The distance at which the created wound was closed by the cells was noted at the 24th hour. Control 48 h (**C**) The distance at which the created wound was closed by the cells was noted at the 48th hour (Scale Bar: 100 µM). (*A higher resolution / colour version of this figure is available in the electronic copy of the article*).

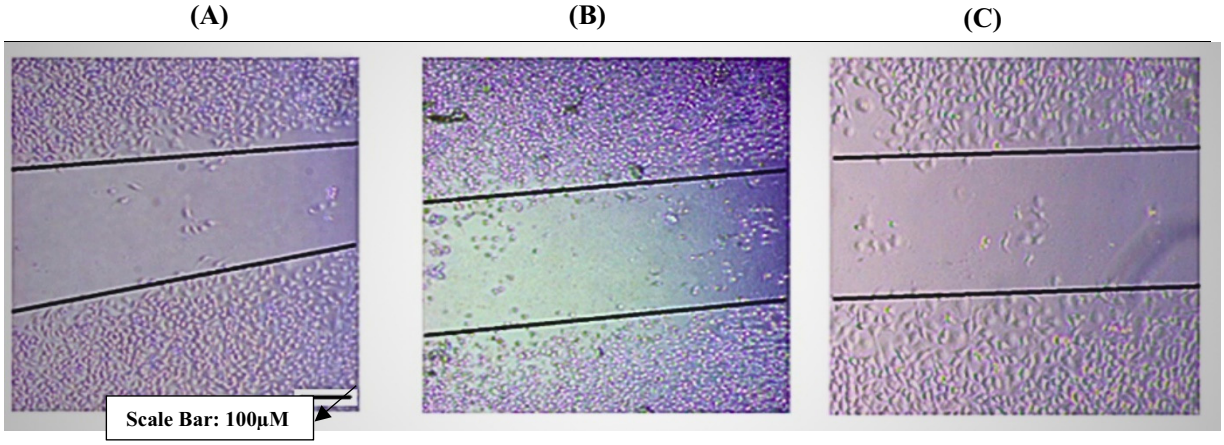

Fig. (4). Irinotecan 48 h (**A**): Irinotecan was applied (48.3 µM) to MDA-MB-231 cell lines and the wound healing amount of the cells was monitored at the 48th hour. Umbelliferone and Irinotecan 48 h (**B**): Combined doses of umbelliferon and irinotecan were applied (20 µM) to MDA-MB-231 cell lines, and the wound healing amount of the cells was monitored at 48 hours. Umbelliferone 48 h (**C**): Umbelliferone was applied (158 µM) to MDA-MB-231 cell lines and the wound healing amount of the cells was monitored at the 48th hour (Scale Bar: 100 µM). (*A higher resolution / colour version of this figure is available in the electronic copy of the article*).

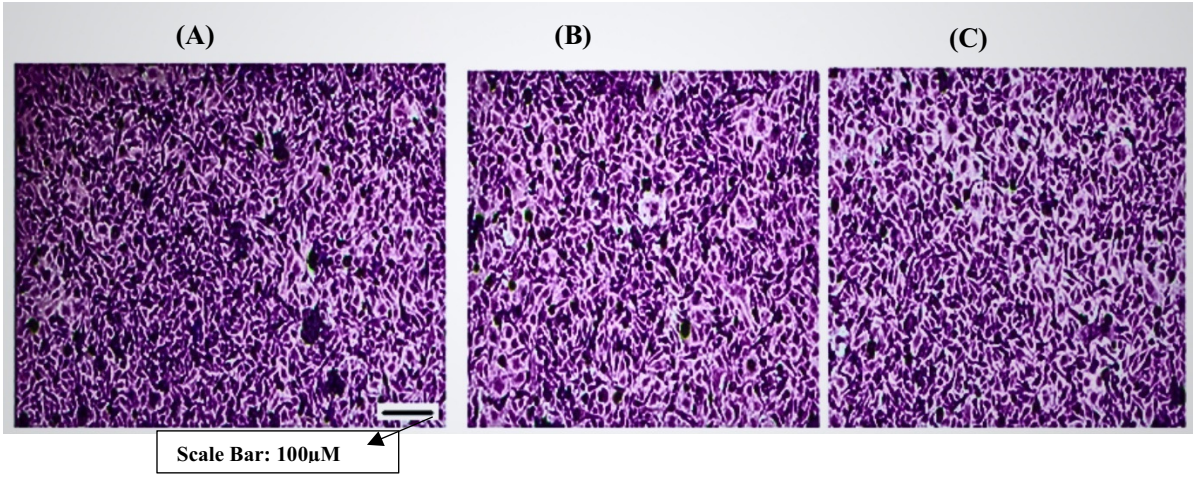

Fig. (5). MDA-MB-231 control (**A**) 24 h: Invasion image of MDA-MB-231 breast cancer cells stained with Giemsa dye at 24 hours. (**B**) 48 h: Invasion image of MDA-MB-231 breast cancer cells stained with Giemsa dye at 48 hours 48 h. (**C**) 72 h: Invasion image of MDA-MB-231 breast cancer cells stained with Giemsa dye at 72 hours. (*A higher resolution / colour version of this figure is available in the electronic copy of the article*).

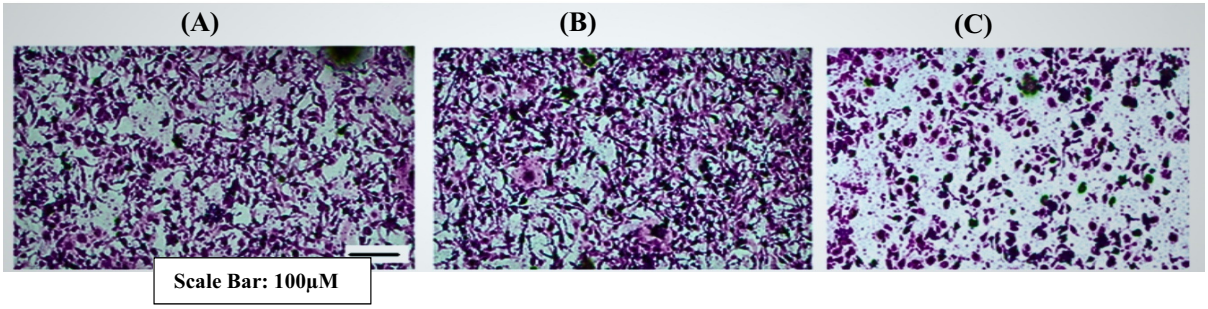

Fig. (6). (**A**) Irinotecan: Invasion image of MDA-MB-231 cell lines applied with 48.3 µM irinotecan at the end of the 48th hour. (**B**) Umbelliferone: Invasion image of MDA-MB-231 cell lines applied with 158 µM umbelliferone at the end of the 48th hour. (**C**) Irinotecan and Umbelliferone Invasion image of MDA-MB-231 cell lines applied with 20 µM umbelliferone and irinotecan at the end of the 48th hour. (Scale Bar: 100 µM). (*A higher resolution / colour version of this figure is available in the electronic copy of the article*).

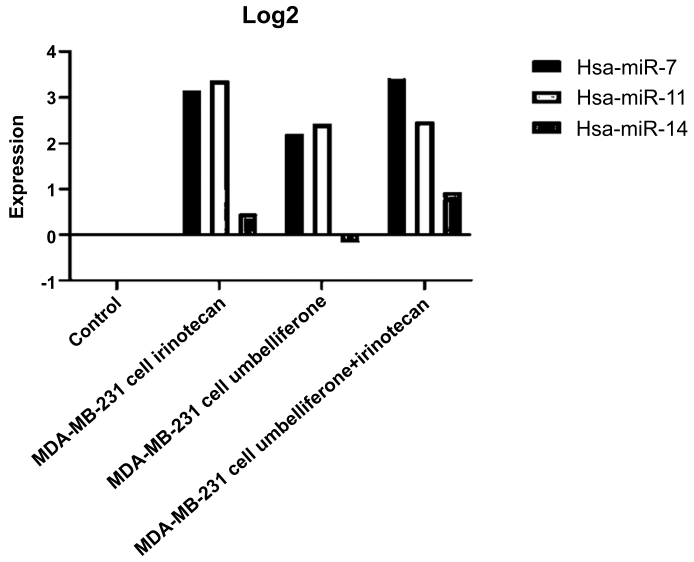

Fig. (7). Expression levels of Hsa-miR-7, Hsa-miR-11, and Hsa-miR-14 in MDA-MB-231 cell line. (*A higher resolution / colour version of this figure is available in the electronic copy of the article*).

Table 3. a: Hsa-miR-7-5p (*H. sapiens* miR-7-5p) sequence, b: The Two-dimensional structure of Hsa-miR-7 (http://rtools.cbrc.jp/centroidfold/index.cgi?query=%3EmiR-7%0D%0AgcggtggaagactagtgattGTCGTATCCAGTGCAGGGTCCGAGGTATTCGCACTGGATACGACacaacaGTGCAGGGTCCGAGG&model_str_1=CONTRAfold&gamma_1=4&req_id=1bc399fa0df1489e184896015352307b11edd9c8), c: The three-dimensional structure of Hsa-miR-5p (https://rnacomposer.cs.put.poznan.pl) was prepared using the Discovery studio visualizer program.

Hsa-miR-7-5p Sequence (a)	Hsa-miR-7-5p two-dimensional Structure (b)	Hsa-miR-7-5p Three-dimensional Structure (c)
Hsa-miR-7-ST: GTCGTATCCAGTG-CAGGGTCCGAGGTATTCGCACTGGATAC-GACacaaca Univ-R: GTGCAGGGTCCGAGG Forwad: gcggtggaagactagtgatt	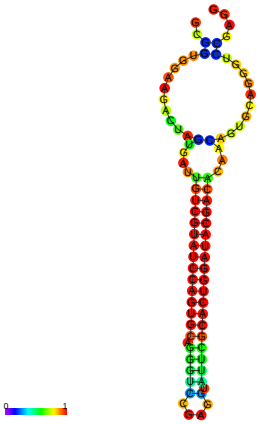	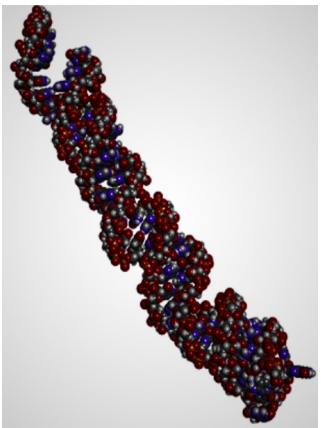

Table 4. **a: Hsa-miR-11(*H. sapiens* miR-11) sequence, b: The Two-dimensional structure of Hsa-miR-11 (http://rtools.cbrc.jp/centroidfold/index.cgi?query=%3EmiR-11%0D%0AgcggcaagaactttctctgtGTCGTATCCAGTGCAGGGTCCGAGGTATTCGCACTGGATACGACcgggtcGTGCAGGGTCCGAGG&model_str_1=BL&gamma_1=4&req_id=0f64ae11c12d3b6a257365cd9896bfc09688e4af), c: The three-dimensional structure of Hsa-miR-11 (https://rnacomposer.cs.put.poznan.pl) was prepared using Discovery Studio Visualizer.**

Hsa-miR-11 Sequence (a)	Hsa-miR-11 Two-dimensional Structure (b)	Hsa-miR-11 Three-dimensional Structure (b)
Hsa-miR-11-ST: GTCGTATCCAGTGCAGGGTCCGAGGTATTCG-CACTGGATACGACcgggtc Univ-R: GTGCAGGGTCCGAGG Forwad: gcggcaagaactttctctgt	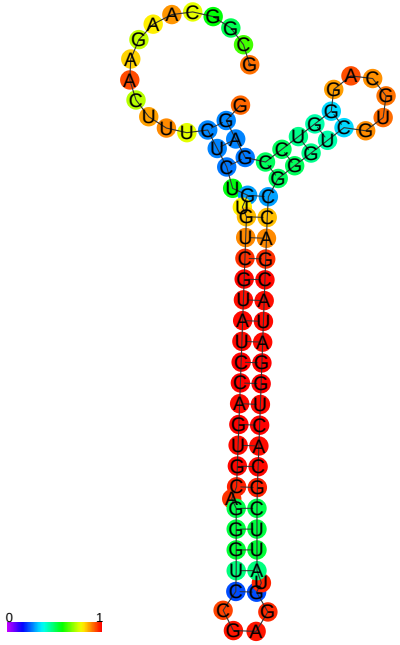	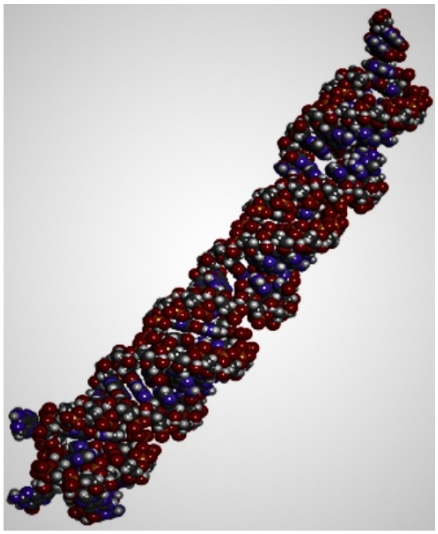

Table 5. **a: Hsa-miR-14 (*H. sapiens* miR-14) sequence, b: The Two-dimensional structure of Hsa-miR-14 (http://rtools.cbrc.jp/centroidfold/index.cgi?query=%3EmiR-14%0D%0Agcgggggagcgagacgggga GTCGTATCCAGTGCAGGGTCCGAGGTATTCGCACTGGATACGACagtgagGTGCAGGGTCCGAGG&model_str_1=CONTRAfold&gamma_1=4&req_id=6efb6b5c92130fa8626e09e7d59f64adf3e1a5cf), c: The Three-dimensional structure of Hsa-miR-14 (https://rnacomposer.cs.put.poznan.pl) was prepared using Discovery Studio Visualizer.**

Hsa-miR-14 Sequence (a)	Hsa-miR-14 Two-dimensional Structure (b)	Hsa-miR-14 Three-dimensional Structure (c)
Hsa-miR-14-ST: GTCGTATCCAGTG-CAGGGTCCGAGGTATTCGCACTGGA-TACGACagtgag Univ-R: GTGCAGGGTCCGAGG Forwad: gcgggggagcgagacgggga	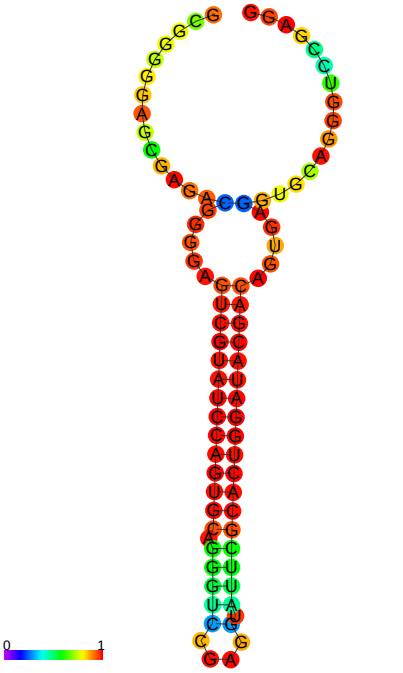	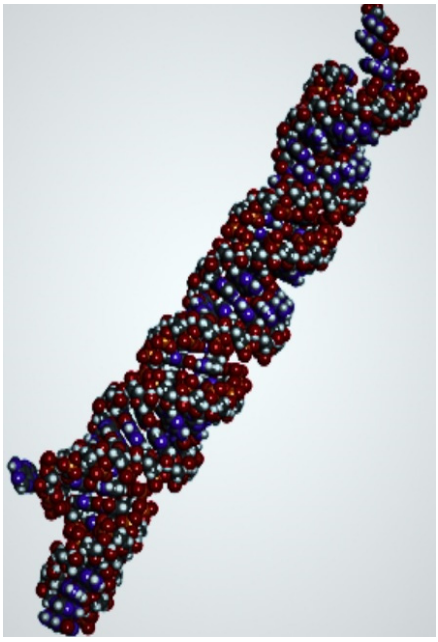

Table 6. Proteins used in molecular docking studies, their PDB (Protein Data Bank) ID codes, and Uniprot names with the three-dimensional structure.

Name of Protein (*H. sapiens*)	PDB ID Code	The Three-dimensional Structure of Protein	Name of Protein (*D. melanogaster*)	Uniprot Name	The Three-dimensional Structure of Protein
Bcl-2	1G5M		BUFFY	AT16536p	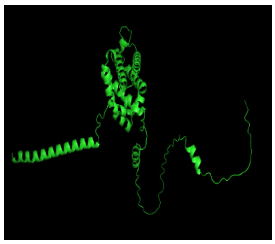
Akt-1	1H10	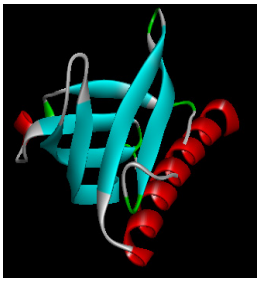	dAKT1	RAC serine/threonine-protein kinase [38] (Dakt1)	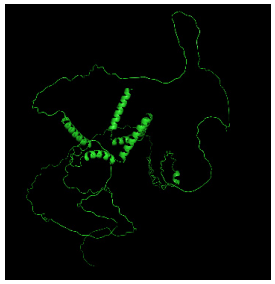
BAD	1G5J		CG15530	AT23209p	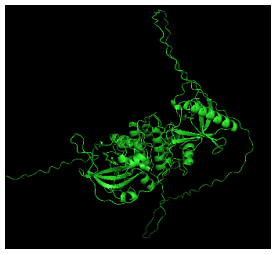

Table 7. The binding energy of umbelliferon and irinotecan to Hsa-miR-7, Hsa-miR-11, and Hsa-miR-14 miRNA molecules.

S. No.	miRNA	Ligand	Binding Energy (kcal/mol) (Autodock Vina)	Binding Position
1	Hsa-miR-7-5p	Umbelliferone	L_1: -7,1	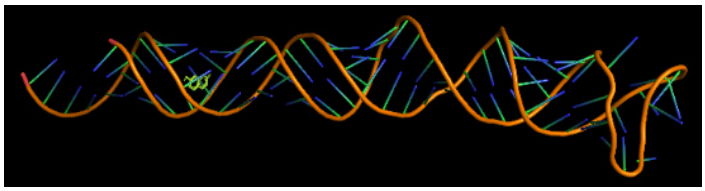
		Irinotecan	L_1: -13,5	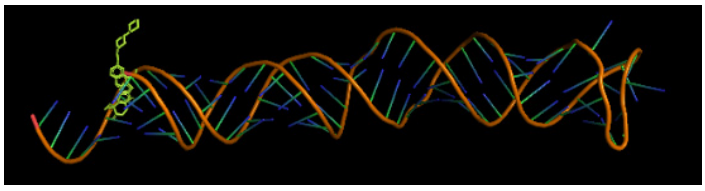
2	Hsa-miR-11	Umbelliferone	L_1: -6,5	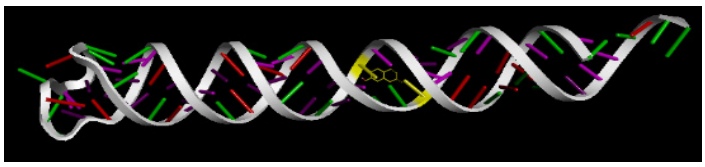

(Table 7) Contd….

S. No.	miRNA	Ligand	Binding Energy (kcal/mol) (Autodock Vina)	Binding Position
-	-	Irinotecan	L_1: -9,4	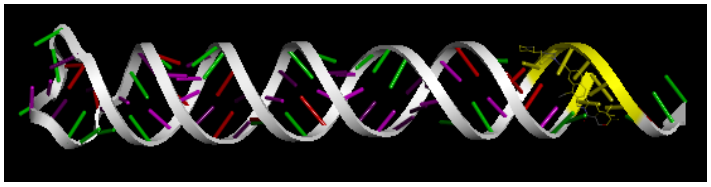
3	Hsa-miR-14	Umbelliferone	L_1: -7,3	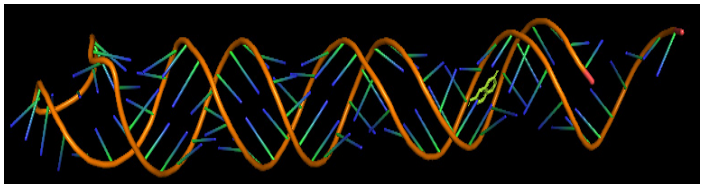
		Irinotecan	L_1: -10,5	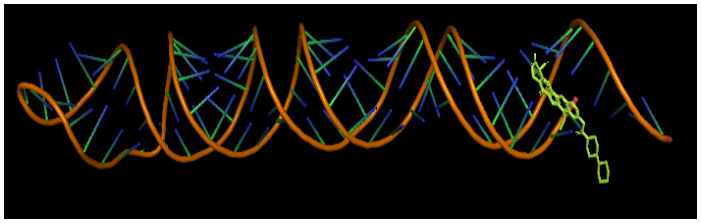

Table 8. Bcl-2 (1G5M), Akt1 (1H10), BAD (1G5J), BUFFY (AT16536p), dAkt1 (RAC serine/threonine-protein kinase), CG15530 (AT23209p), The binding energy of proteins to umbelliferon and irinotecan.

S. No.	Protein *(H.sapiens)*	Ligand	Binding Energy (Autodock Vina) (kcal/mol)	Swissdock Program (kcal/mol)	Seamdock Program (kcal/mol)	Binding Position Autodock Vina	Protein *(D. melanogaster)*	Ligand	Binding Energy (Autodock Vina) (kcal/mol)	Seamdock Program (kcal/mol)	Binding Position Autodock Vina
1	Bcl-2 (1G5M)	Umbelliferon	-6,1	6,31	-5,9	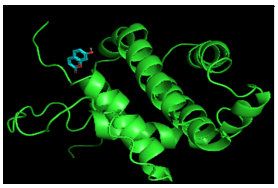	BUFFY	Umbelliferon	-4,7	-4,7	
		İrinotekan	-9,2	-8,5	-9,1	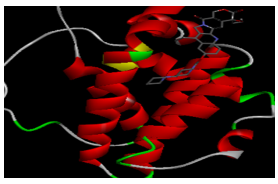		Irinotekan	-8,3	-7,8	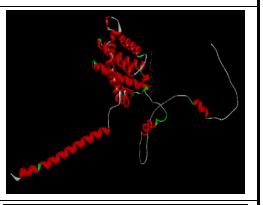
2	Akt1 (1H10)	Umbelliferon	-5,6	-6,27	-5,4	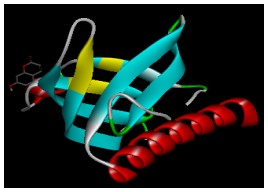	dAkt1	Umbelliferon	-6,4	-6,3	

(Table 8) Contd….

S. No.	Protein *(H.sapiens)*	Ligand	Binding Energy (Autodock Vina) (kcal/mol)	Swissdock Program (kcal/mol)	Seamdock Program (kcal/mol)	Binding Position Autodock Vina	Protein *(D. melanogaster)*	Ligand	Binding Energy (Autodock Vina) (kcal/mol)	Seamdock Program (kcal/mol)	Binding Position Autodock Vina
-	-	İrinotekan	-8,4	-7,01	-8,3	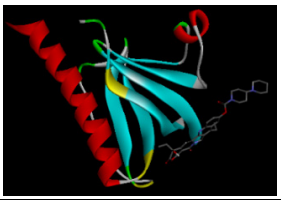	-	Irinotekan	-11,3	-9,4	
3	BAD (1G5J)	Umbelliferon	-6,9	-6,52	-6,7	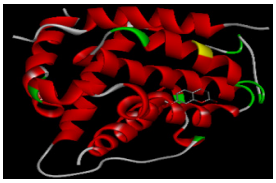	CG15530	Umbelliferon	-5,0	-5,1	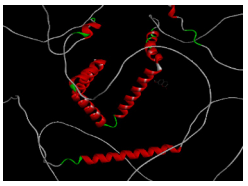
		İrinotekan	-9,3	-7,9	-8,2	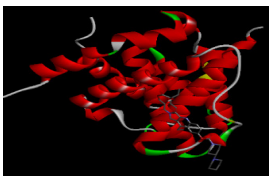		Irinotekan	-8,5	-7,9	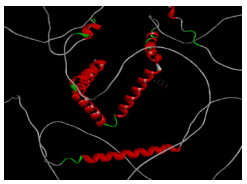

umbelliferone, irinotecan, and drug combinations to Bcl-2 (1G5M), Akt1 (1H10), and BAD (1G5J) proteins are shown in Table **9**.

The binding energies of umbelliferon and irinotecan to *D .melanogaster* proteins were calculated using Autodock vina and Seamdock programs. The binding energies of umbelliferone, irinotecan, and drug combinations to BUFFY (AT16536p), dAkt1 (RAC serine/threonine-protein kinase), CG15530 (AT23209p) proteins are shown in Table **10**.

The binding positions and hydrogen bonds of umbelliferon and irinotecan to *H. sapiens* proteins are shown in Table **11**.

3.6. ADME/T Analyses

The drug potential of umbelliferon and irinotecan was calculated with the SwissADME online program.

As a result of the ADME/T analysis, it was found that the properties of umbelliferone, such as molecular weight, polarity, insolubility, flexibility, and oil solubility, were within the specified range.

According to the drug-likeness analysis, Umbelliferone was identified as consistent with Lipinski's, Veber's, or Ghose's rules.

Following Lipinski's rule (often referred to as Pfizer's rule or Lipinski's rule of five), an active drug should have no more than one violation of the following properties: molecular weight (MW) ≤ 500, LogP ≤ 5, hydrogen bond acceptors ≤ 10, and hydrogen bond donors ≤ 5. According to Veber's rules, an active drug should have a total of hydrogen bonds ≤ 12, rotatable bonds ≤ 10, and a polar surface area (PSA) ≤ 140, which tends to result in oral bioavailability ≥ 20%. Following Ghose's rules, an active drug should have properties such as Log P (− 0.4~5.6), Molar refractivity (40~150), MW (160~480), the number of atoms (20~70), and a polar surface area (PSA) < 140 [40-42]. As a result of the drug similarity analysis, it is seen that Umbelliferon complies with the rules of Lieber, Weber, and Ghose. ADME/T analysis of umbelliferone is shown in Fig. (**8**).

3.7. Molecular Dynamics Analyses

For molecular dynamics research, the BAD protein was selected. Table **12** displays the BAD (PDB İD: 1G5J) protein's single, umbelliferon-bound, and combined drug-bound dynamic investigations. Graphs that display the stability of a complex structure at a given time are called root mean square deviations, or RMSDs. The distribution of a structure's atoms along an axis is known as its radius of gyration (Rg). Rg graphs provide details regarding the structure's compactness. The chemical and physical characteristics of matter are mostly determined by hydrogen bonding [43].

The BAD protein's RMSD (Root mean square deviation) value was steady at around 0.25 nm throughout our investigation. The stability of the BAD and umbelliferone combination declined after 35 ns, while it remained constant for around 0.5 nm. The BAD-Irinotecan and umbelliferone complex exhibits varied initial stability. Stability was attained at about 0.58 nm after 35 ns. The BAD protein has an average Rg (Radius of gyration) value of around 1.65 in the Rg simulation research. The BAD and umbelliferone complex has an average Rg value of around 1.65 nm. The average value was around 2 nm after 35 ns. The BAD irinotecan and umbelliferone complex had an estimated Rg value of 1.65 nm, but after 35 ns, the average Rg value was 1.60 nm. According to hydrogen bond analysis, an increase in the number of bonds is correlated with a decrease in the energy of pharmacological systems. It is evident that the BAD-irinotecan+umbelliferone complex and the BAD protein have greater average energies than the BAD-umbelliferone complex. This might suggest that compared to other compounds, the BAD+umbelliferone combination has a better solubilization impact.

Table 9. Comparison of the binding energy of the second ligand-free to the protein-ligand complex and the single binding energy of the ligand.

Receptor	Ligand	Audock Vina (Kcal/mol)	Seamdock (Kcal/mol)	Receptor-ligand Complex	Second Ligand	Swissdock (Kcal/mol)	Seamdock (Kcal/mol)
Bcl-2 (1G5M)	Umbelliferon	-6,1	-6,31	Bcl-2 (1G5M)+irinotecan	Umbelliferon	-5,9	-5,9
Bcl-2 (1G5M)	Irinotecan	-10,7	-9,1	Bcl2(1G5M)+Umbelliferon	Irinotecan	-8,53	-8,9
Akt1 (1H10)	Umbelliferon	-5,6	-5,4	Akt1 (1H10)+Irinotecan	Umbelliferon	-5,9	-5,4
Akt1 (1H10)	Irinotecan	-8,4	-8,3	Akt1(1H10)+Umbelliferon	Irinotecan	-6,92	-7,8
BAD (1G5J)	Umbelliferon	-6,9	-6,7	BAD (1G5J)+Irinotecan	Umbelliferon	-6,62	-6,7
BAD (1G5J)	Irinotecan	-9,3	-8,2	BAD (1G5J)+Umbelliferon	Irinotecan	-7,7	-8,5

Table 10. Comparison of the binding energy of the second ligand-free to the *D.melanogaster* protein-ligand complex and the single binding energy of the ligand.

Receptor	Ligand	Audock Vina (Kcal/mol)	Seamdock (Kcal/mol)	Receptor-ligand Complex	Second Ligand	Audock Vina (Kcal/mol)	Seamdock (Kcal/mol)
BUFFY	Irinotecan	-8,3	-7,8	BUFFY+Umbelliferone	Irinotecan	-8,0	-7,2
BUFFY	Umbelliferone	-4,7	-4,7	BUFFY+Irinotecan	Umbelliferone	-4,1	-4,5
CG15530	Irinotecan	-8,5	-7,9	CG15530+Umbelliferone	Irinotecan	-9,5	-8,0
CG15530	Umbelliferone	-5,0	-5,1	CG15530+Irinotecan	Umbelliferone	-5,2	-5,1
Akt1	Irinotecan	-11,3	-9,4	Akt1+Umbelliferone	Irinotecan	-10,4	-9,2
Akt1	Umbelliferon	-6,4	-6,3	Akt1 + Irinotecan	Umbelliferone	-6,4	-6,2

Table 11. The binding position and the number of hydrogen bonds of umbelliferone and irinotecan with Bcl2, BAD, and Akt1 proteins.

Protein-ligand Complex	Binding Position	Number of Hydrogen Bonds
BAD (PDB İd: 1G5J)-Umbelliferon	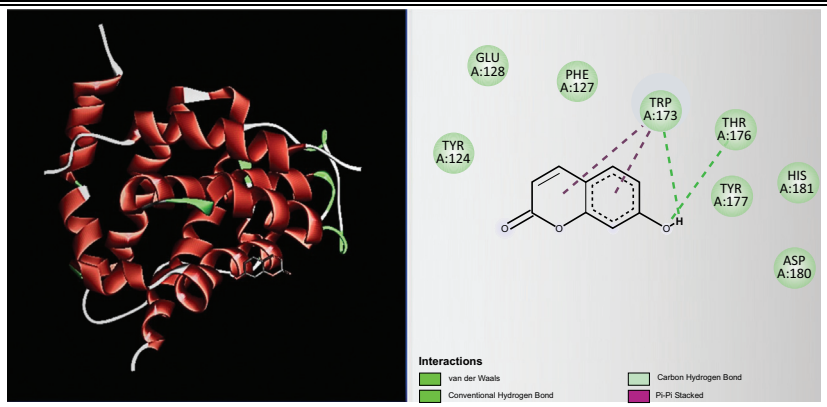	2 Hydrogen Bonds: TRP (A:173)
BAD (PDB İd: 1G5J)-Irinotecan	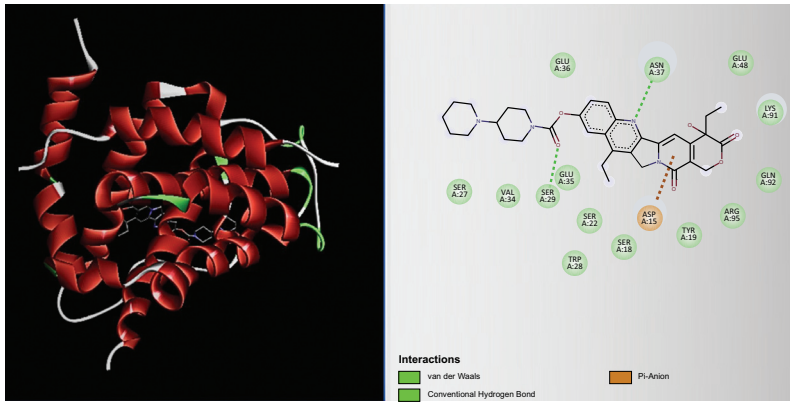	2 Hydrogen Bonds ASN (A:37), SER (A:29)

(Table 11) Contd….

Protein-ligand Complex	Binding Position	Number of Hydrogen Bonds
(BAD (PDB İd: 1G5J)-Umbelliferon) + Irinotecan	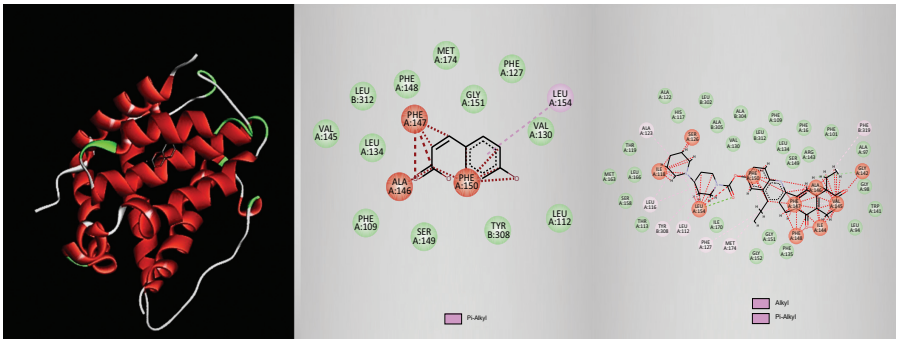	BAD-Umb; No hydrogen bonds BAD-Irinotecan; 2 Hydrogen Bonds ASN (A:37), SER (A:29)
(BAD (PDB İd: 1G5J)-Irinotecan) + umbelliferon	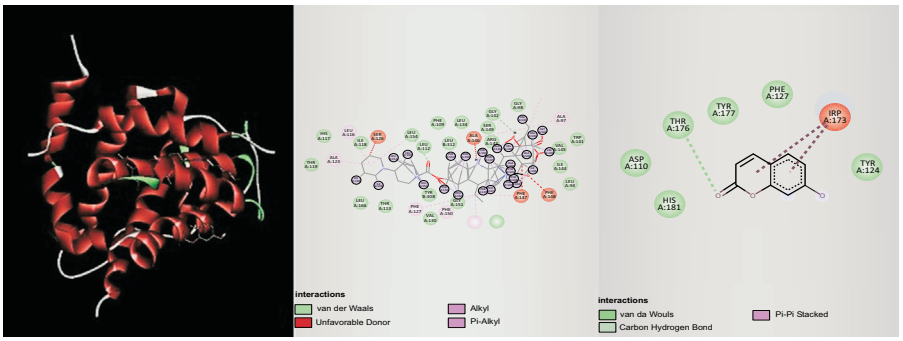	BAD-Umbelliferon: No hydrogen bonds BAD-Irinotecan: 2 Hydrogen Bonds LEU (A:154), GLY (A:142)
Bcl-2 (PDB İd: 1G5M) - Umbelliferon	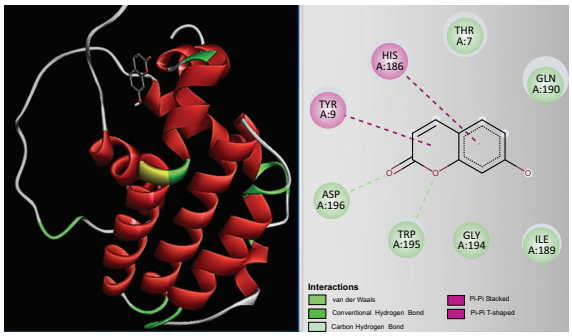	2 Hydrogen Bonds ASP (A:196), TRP (A:195)
Bcl-2(PDB İd: 1G5M)-Irinotecan	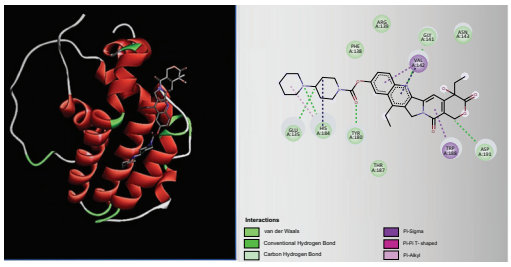	1 Hydrogen Bonds TRY (A:180)
(Bcl-2(PDB İd: 1G5M)-Umbelliferon) + Irinotecan	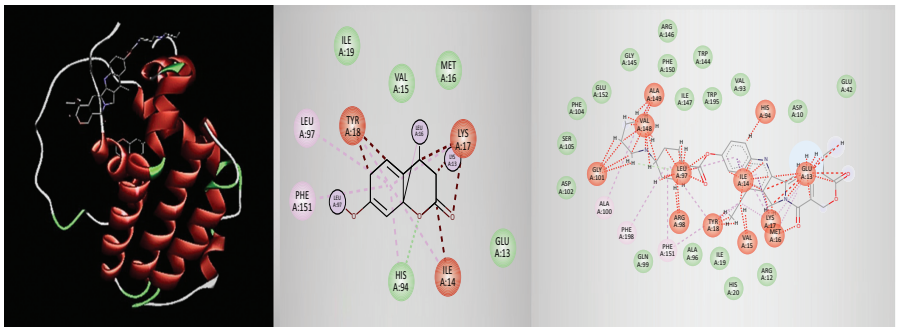	Bcl2- Umbelliferon: 1 Hydrogen Bonds: HIS (A:94) Bcl2-Irinotecan: 2 Hydrogen Bonds; ASN (A:11), THR (A:7)

(Table 11) Contd….

Protein-ligand Complex	Binding Position	Number of Hydrogen Bonds
(Bcl-2(PDB İd: 1G5M)-Irinotecan) + Umbelliferon	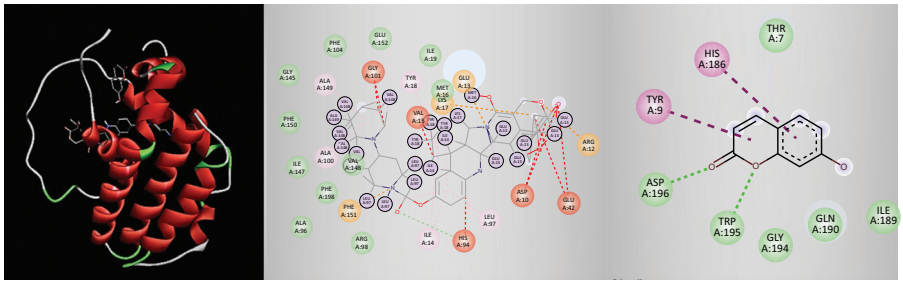	Bcl2-Irinotecan: 1 Hydrogen Bonds, HİS (A:94), Bcl2-Umbelliferon: 2 Hydrogen Bonds: ASP (A:196), TRP (A:195)

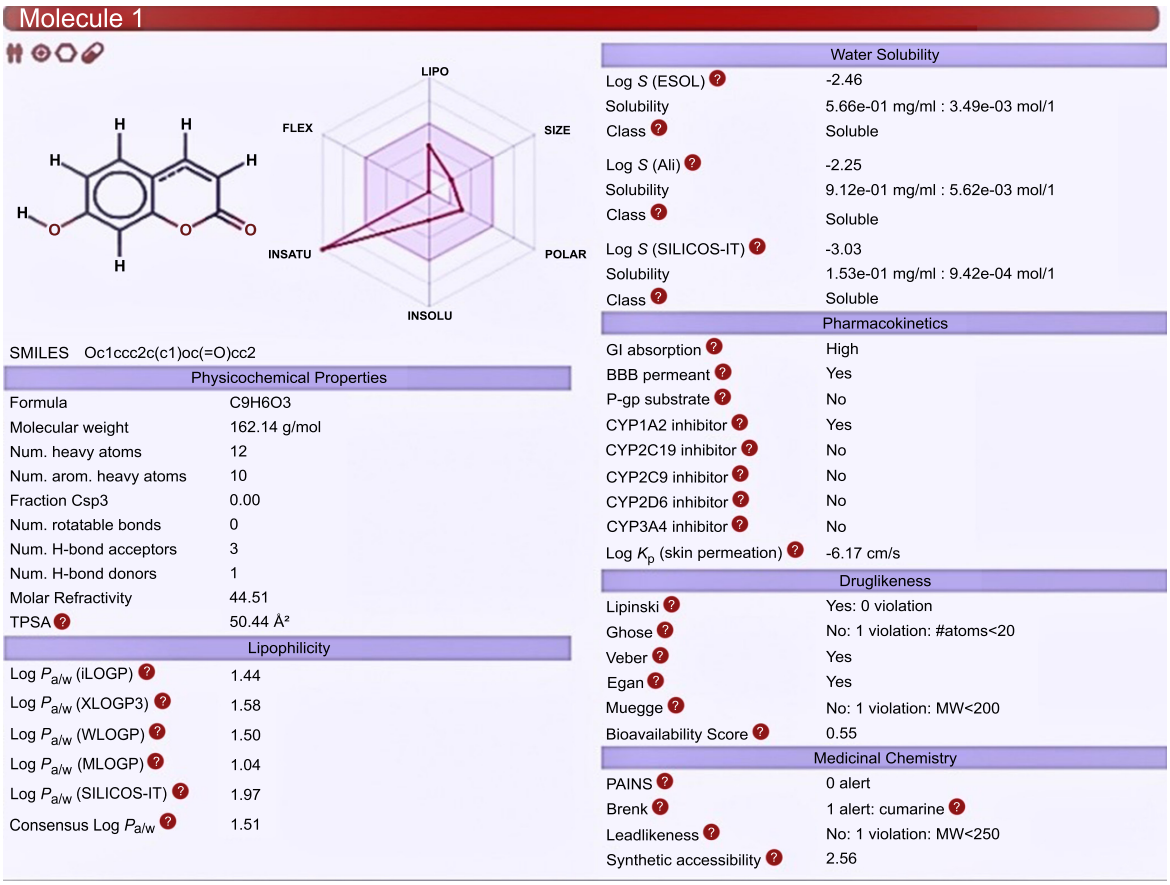

Fig. (8). Table showing ADME/T analysis of umbelliferone (SIZE: Molecular weight, POLAR: Polarity, INSOLU: Indissolubility, İNSATU: Saturation, FLEX: Flexibility, LIPO: Lipophilicity). (*A higher resolution / colour version of this figure is available in the electronic copy of the article*).

4. DISCUSSION

In this study, the cytotoxic effects of irinotecan [8], a cytotoxic drug used for cancer treatments, and umbelliferone, which is known to have curative effects on diseases such as bacterial diarrhea, dysentery, leucoderma, and fungi, especially in viral therapies [21], were investigated on *D. melanogaster* and MDA-MB-231 breast cancer cell lines. *In vivo*, *in vitro,* and *in silico* analyses were performed. The expression levels of umbelliferon and irinotecan, miR-7, miR-11, and miR-14 were investigated, and molecular docking studies were conducted to calculate the binding energies of the drugs to both the proteins associated with apoptosis and the miRNAs in question. In the studies, the cytotoxic effects of the drugs on MDA-MB-231 cell lines and the model organism *D. melanogaster* were studied, and their effective doses were determined.

D. melanogaster, a model organism that has been frequently used in recent years, is extremely important in terms of signaling pathways that cause apoptosis, genes that cause tumor formation, and evolutionarily conserved genes that are orthologous to human genes.

GBM (glioblastoma), one of the most common brain tumors, occurs as a result of mutations in the PI3K signaling pathway and EGFR tyrosine kinase receptors. The cellular origin of GBM was found through studies on the model organism *D. melanogaster* [44]. Signal transduction pathways such as EGFR/RTK-Ras, PI3K, Notch, Wnt, Jak-STAT, Hedhegog, and TGF-β, which are thought to be evolutionarily conserved, were found as a result of studies conducted on the model organism *D. melanogaster.* Likewise, dPTEN found in *D. melanogaster* is the homolog of PTEN, which

Table 12. Molecular dynamic studies of BAD, BAD-Umbelliferone, BAD-Irinotecan+Umbelliferon.

	Radius of Gyration(Rg)	Root Mean Square Deviation (RMSD)	Hydrogen Bond (HB)
BAD (ID: 1G5J)	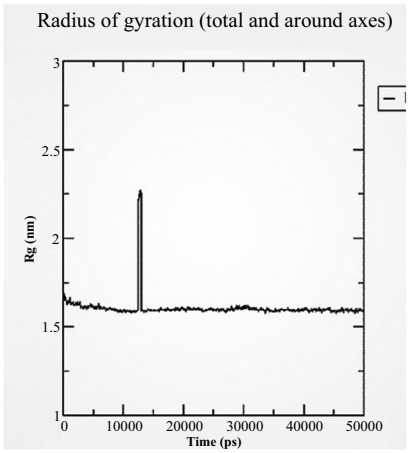	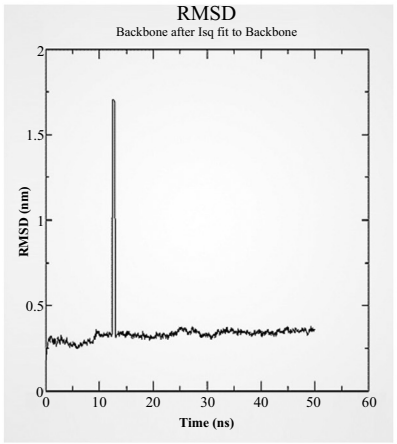	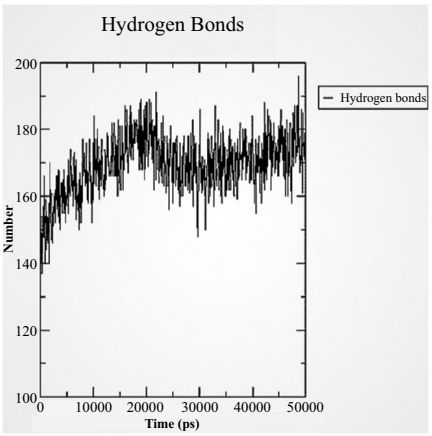
	Radius of gyration(Rg)	Root mean square deviation (RMSD)	Hydrogen Bond (HB)
BAD (ID: 1G5J) + Umbelliferone	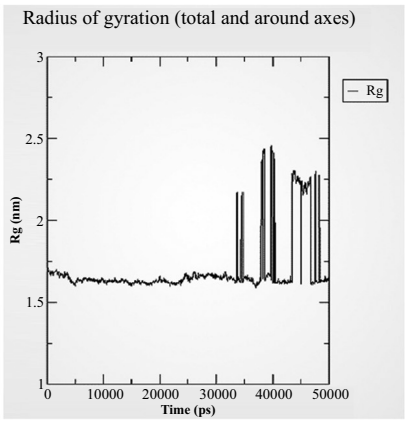	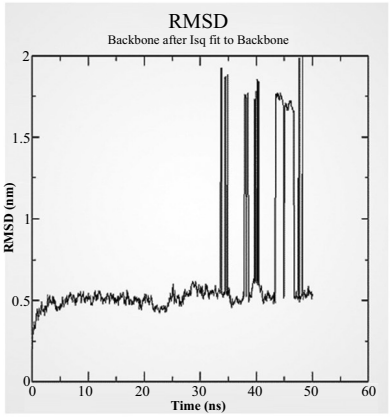	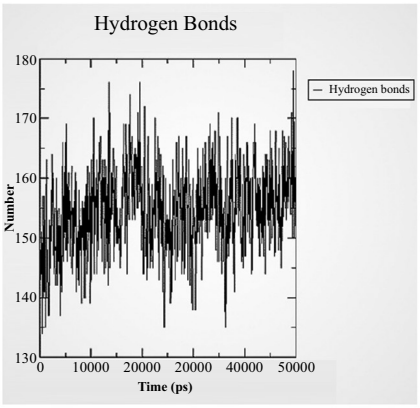
	Radius of gyration(Rg)	Root mean square deviation (RMSD)	Hydrogen Bond (HB)
[BAD (ID: 1G5J) – Irinotecan] + Umbelliferone	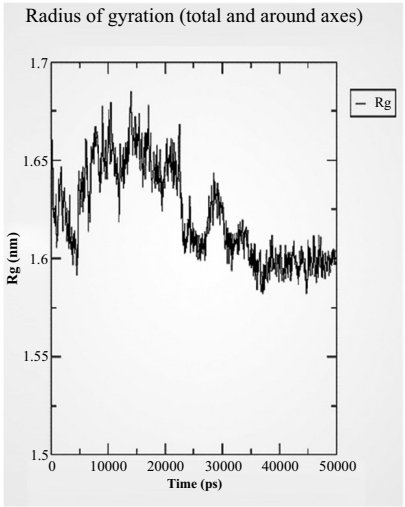	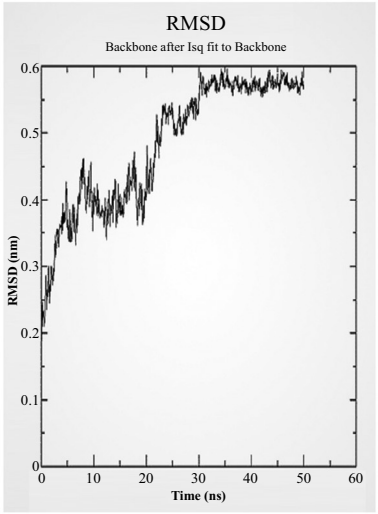	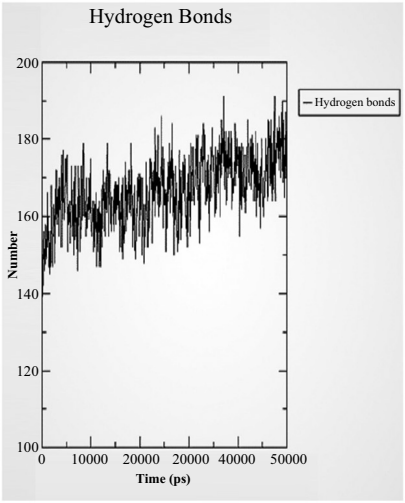

functions as a tumor suppressor gene in mammals [2]. PI3K phosphorylation activates 4,5-bisphosphate (PIP2), which in turn activates the second messenger phosphatidylinositol 3,4,5-triphosphate (PIP3). The PIP3 receptor activates serine/threonine kinase, Akt, and PDK1, which control various receptors in regulating cell cycle progression, cell death, and protein synthesis. Studies conducted on *D. melanogaster* reveal that this transmission pathway has an important role in the control of general growth [2, 45]. The first examples of tumor suppressor genes were discovered thanks to *D. melanogaster* [46, 47]. These examples show the importance of the model organism *D. melanogaster* in cancer research.

In the wound healing experiment, the spread of cells is seen at the end of the 48 hours. In addition, this progress has been limited

in umbelliferon, irinotecan, and drug combinations. It is a situation that should be taken into consideration, especially when the cells to which drug combinations are applied die to a large extent. In the invasion experiment, the invasive behavior of the cells was restricted compared to the control group. It can be understood from the dying cells that invasion is prevented more, especially in drug combinations.

As a result of expression analyses, a significant increase in hsa-miR-7, hsa-miR-14, and hsa-miR-11 expressions was observed in cells treated with umbelliferon and irinotecan - compared to the control groups ($p < 0.05$). However, it was determined that miRNA expression levels decreased when umbelliferon and irinotecan were treated together ($p < 0.05$). miR-14 is a miRNA with known antiapoptotic properties [48-50]. In fact, human miR-11 and miR-14 are miRNAs that have recently entered the literature. Although they are not yet available on RNA data sites, they are available on NCBI data accumulation sites.

In separate and combinational applications, the increase in the expression of miR-7 [51], which is known to cause tumor formation, is remarkable. Another issue that needs to be taken into consideration is the downregulation of gene expression levels by combinatorial doses of molecules.

In previous studies, miR-7 is abundantly expressed in the human brain, spleen, and pancreas, while its expression is less in other tissues [52-54]. It has been explained that miR-7, which suppresses the genes regulating KLF4 (Kruppel-Like-Factor) expression, limits the metastasis capacity of cells [50, 52]. Additionally, studies have shown that it binds to the RAF1 molecule, reducing its activity, and as a result, it has an antitumor effect [51, 53].

In another study, it was found that high expression of miR-7 led to the suppression of MRP1 and Bcl-2 and enhanced the response to chemotherapy [53, 55]. Based on these studies, the changes observed in the expression levels of miR-7, which generally functions as a tumor suppressor, in single and combination doses of irinotecan and umbelliferone, especially in the MDA-MB-231 breast cancer cell line, are important.

Moreover, the fact that irinotecan, umbelliferon, and drug combination (umbelliferon and irinotecan) inhibit the invasion and migration of MDA-MB-231 cells is an important indicator for the anticarcinogenic effects of chemicals.

Another issue as important as the effect of drugs on expression levels is the binding energies of chemical agents to target proteins and miRNAs. As a result of *in silico* analyses, binding energies and binding positions of umbelliferon and irinotecan to target molecules in single and combinational doses were found, and amino acids and hydrogen bonds at the binding points were determined.

In the docking studies, the binding energy of umbelliferon, irinotecan and their combination with Bcl2, one of the anti-apoptotic proteins, was determined. As a result of the analysis, umbelliferon and irinotecan bound to Bcl-2 protein with high energy. In docking studies, the binding energy of umbelliferon and irinotecan to Akt1 protein at single and combination doses was determined. It has been observed that the two chemical agents bind with high binding energy. In particular, the binding energy of irinotecan is extremely high. Akt protein is closely associated with cancer formation and resistance to chemotherapy [56]. For this reason, the high binding energy of drugs to the Akt protein is extremely important for the progress of chemotherapy and the prevention of cancer formation. Furthermore, in the study, the binding energy of umbelliferon and irinotecan to the BAD protein was calculated, and it was revealed that both chemical agents were bound to the protein with high binding energy. When examining the impact of combined drugs on *Drosophila* and conducting docking studies, it is necessary to consider the entirety of the findings. Specifically, the lower binding energy of combined applications on apoptotic proteins like Akt1 and BUFFY indicates a reduced toxic effect. Our study is supported by *in vivo* research on *Drosophila* larvae, which confirms the diminished toxicity of drug combinations. However, previous studies suggest that single use of drugs may lead to increased toxicity [10, 57].

In vivo studies conducted on *D. melanogaster* larvae provide important information about the toxicity of drugs. As in our study, *D. melanogaster* is preferred as a model organism in many cancer studies. Cancer occurs in many steps, such as loss of function of tumor suppressor genes and activation of oncological pathways. The evolutionary conservation of these signaling pathways, which are similar to humans, in *D. melanogaster* and the ease of their genetic analysis are the greatest strengths of this model organism. *D. melanogaster* has been used extensively in cancer research, particularly in the past 10 years, and this is highly crucial [58].

Additionally, in these studies, miRNAs with both apoptotic and anti-apoptotic properties were selected. The effect of single and combined doses of these two chemicals on the expression levels of different proteins stands out as an issue that needs to be investigated in future studies.

CONCLUSION

In our study, it can be concluded that the cytotoxic effects of individual and combination doses of umbelliferon and irinotecan on MDA-MB-231 breast cancer cells and *D. melanogaster* larvae are significant. In addition, the effects of umbelliferone and irinotecan on the expression level of miR-7, which is common to *D. melanogaster* and human miRNAs, should be widely investigated. Expression analysis and docking studies of hsa-miR-11 and hsa-miR-14, which have been newly studied and are not available in data repositories, are important for cancer research. In particular, the expression and binding energy of these miRNAs in new drug combinations and the expression level in different cancer cell lines are important for future studies. Another crucial point is that *in vivo* tests using different model species validate the usage of drugs at both single and mixed dosages.

AUTHORS' CONTRIBUTIONS

The authors confirm their contribution to the paper as follows: A.T., S.Y., and F.E. contributed to the study conception and design. E.T. wrote the paper. E.T., S.Y. and F.E. collected the data. All authors reviewed the results and approved the final version of the manuscript.

LIST OF ABBREVIATIONS

FAC = Fluorouracil, and Cyclophosphamide

FBS = Fetal Bovine Serum

MW = Molecular Weight

PSA = Polar Surface Area

ETHICS APPROVAL AND CONSENT TO PARTICIPATE

Not applicable.

HUMAN AND ANIMAL RIGHTS

Not applicable.

CONSENT FOR PUBLICATION

Not applicable.

AVAILABILITY OF DATA AND MATERIALS

The data and supportive information are available within the article.

FUNDING

This study was financially supported by the Erciyes University Research Fund (project no: FDK-2021-11191). This study was conducted in the cancer pharmacology laboratory of Kırşehir Ahi Evran University Faculty of Medicine.

CONFLICT OF INTEREST

The authors declare no conflict of interest, financial or otherwise.

ACKNOWLEDGEMENTS

We would like to thank the Proofreading & Editing Office of the Dean for Research at Erciyes University for the copyediting and proofreading service for this manuscript.

REFERENCES

[1] Bilder, D. Epithelial polarity and proliferation control: links from the *Drosophila* neoplastic tumor suppressors. *Genes Dev.,* **2004**, *18*(16), 1909-1925. http://dx.doi.org/10.1101/gad.1211604 PMID: 15314019

[2] Gao, X.; Neufeld, T.P.; Pan, D. *Drosophila* PTEN regulates cell growth and proliferation through PI3K-dependent and -independent pathways. *Dev. Biol.,* **2000**, *221*(2), 404-418. http://dx.doi.org/10.1006/dbio.2000.9680 PMID: 10790335

[3] Mehlen, P.; Puisieux, A. Metastasis: A question of life or death. *Nat. Rev. Cancer,* **2006**, *6*(6), 449-458. http://dx.doi.org/10.1038/nrc1886 PMID: 16723991

[4] Milne, A.N.; Carneiro, F.; O'Morain, C.; Offerhaus, G.J.A. Nature meets nurture: Molecular genetics of gastric cancer. *Hum. Genet.,* **2009**, *126*(5), 615-628. http://dx.doi.org/10.1007/s00439-009-0722-x PMID: 19657673

[5] Chabner, B.A.; Roberts, T.G., Jr Chemotherapy and the war on cancer. *Nat. Rev. Cancer,* **2005**, *5*(1), 65-72. http://dx.doi.org/10.1038/nrc1529 PMID: 15630416

[6] Yardley, D.A. Drug resistance and the role of combination chemotherapy in improving patient outcomes. *Int. J. Breast Cancer,* **2013**, *2013*, 1-15. http://dx.doi.org/10.1155/2013/137414 PMID: 23864953

[7] Greenberg, P.A.; Hortobagyi, G.N.; Smith, T.L.; Ziegler, L.D.; Frye, D.K.; Buzdar, A.U. Long-term follow-up of patients with complete remission following combination chemotherapy for metastatic breast cancer. *J. Clin. Oncol.,* **1996**, *14*(8), 2197-2205. http://dx.doi.org/10.1200/JCO.1996.14.8.2197 PMID: 8708708

[8] Bailly, C. Irinotecan: 25 years of cancer treatment. *Pharmacol. Res.,* **2019**, *148*, 104398. http://dx.doi.org/10.1016/j.phrs.2019.104398 PMID: 31415916

[9] Shitara, T.; Shimada, A.; Hanada, R.; Matsunaga, T.; Kawa, K.; Mugishima, H.; Sugimoto, T.; Mimaya, J.; Manabe, A.; Tsurusawa, M.; Tsuchida, Y. Irinotecan for children with relapsed solid tumors. *Pediatr. Hematol. Oncol.,* **2006**, *23*(2), 103-110. http://dx.doi.org/10.1080/08880010500457152 PMID: 16651238

[10] Kciuk, M.; Marciniak, B.; Kontek, R. Irinotecan—still an important player in cancer chemotherapy: A comprehensive overview. *Int. J. Mol. Sci.,* **2020**, *21*(14), 4919. http://dx.doi.org/10.3390/ijms21144919 PMID: 32664667

[11] Hassanein, E.H.M.; Ali, F.E.M.; Sayed, M.M.; Mahmoud, A.R.; Jaber, F.A.; Kotob, M.H.; Abd-Elhamid, T.H. Umbelliferone potentiates intestinal protective effect of *Lactobacillus acidophilus* against methotrexate-induced intestinal injury: Biochemical and histological study. *Tissue Cell,* **2023**, *82*, 102103. http://dx.doi.org/10.1016/j.tice.2023.102103 PMID: 37178526

[12] Choi, G.Y.; Kim, H.B.; Cho, J.M.; Sreelatha, I.; Lee, I.S.; Kweon, H.S.; Sul, S.; Kim, S.A.; Maeng, S.; Park, J.H. Umbelliferone ameliorates memory impairment and enhances hippocampal synaptic plasticity in scopolamine-induced rat model. *Nutrients,* **2023**, *15*(10), 2351. http://dx.doi.org/10.3390/nu15102351 PMID: 37242234

[13] Yu, S.M.; Hu, D.H.; Zhang, J.J. Umbelliferone exhibits anticancer activity *via* the induction of apoptosis and cell cycle arrest in HepG2 hepatocellular carcinoma cells. *Mol. Med. Rep.,* **2015**, *12*(3), 3869-3873. http://dx.doi.org/10.3892/mmr.2015.3797 PMID: 25997538

[14] Shen, J.Q.; Zhang, Z.X.; Shen, C.F.; Liao, J.Z. Anticarcinogenic effect of Umbelliferone in human prostate carcinoma: An *in vitro* study. *J. Balkan Union Oncol.,* **2017**, *22*(1), 94-101. PMID: 28365941

[15] Kumar, V.; Ahmed, D.; Verma, A.; Anwar, F.; Ali, M.; Mujeeb, M. Umbelliferone β-D-galactopyranoside from *Aegle marmelos* (L.) corr. an ethnomedicinal plant with antidiabetic, antihyperlipidemic and antioxidative activity. *BMC Complement. Altern. Med.,* **2013**, *13*(1), 273. http://dx.doi.org/10.1186/1472-6882-13-273 PMID: 24138888

[16] Salam, S.; Velli, S.K.; Krishnan, P.; Selvanathan, I.; Murugan, M.; Subramaniam, N.; Thiruvengadam, D. Anti-cancer efficacy of umbelliferone against benzo (a) pyrene-induced lung carcinogenesis in Swiss albino mice. *MJB,* **2018**, *5*, 79-89.

[17] Irinotecan. **2023**. Available from:https://pubchem.ncbi.nlm.nih.gov/compound/Irinotecan(accessed on 28-9-2024)

[18] Umbelliferone. **2023**. Available from:https://pubchem.ncbi.nlm.nih.gov/compound/Umbelliferone(accessed on 28-9-2024)

[19] Mazimba, O. Umbelliferone: Sources, chemistry and bioactivities review. *Bulletin Faculty Pharm.,* **2017**, *55*, 223-232.

[20] Parhoodeh, P.; Rahmani, M.; Hashim, N.M.; Sukari, M.A.; Cheng Lian, G.E. Lignans and other constituents from aerial parts of *Haplophyllum villosum*. *Molecules,* **2011**, *16*(3), 2268-2273. http://dx.doi.org/10.3390/molecules16032268 PMID: 21383663

[21] Singh, R.; Singh, B.; Singh, S.; Kumar, N.; Kumar, S.; Arora, S. Umbelliferone – An antioxidant isolated from *Acacia nilotica* (L.) Willd. Ex. Del. *Food Chem.,* **2010**, *120*(3), 825-830. http://dx.doi.org/10.1016/j.foodchem.2009.11.022

[22] Rodriguez, L.G.; Wu, X.; Guan, J.L. Wound-healing assay. *Methods Mol. Biol.,* **2005**, *294*, 023-030. http://dx.doi.org/10.1385/1-59259-860-9:023 PMID: 15576902

[23] Shaw, L.M. Tumor cell invasion assays. *Methods Mol. Biol.,* **2005**, *294*, 097-106. http://dx.doi.org/10.1385/1-59259-860-9:097 PMID: 15576908

[24] Atli, E.; Tamtürk, E. Investigation of developmental and reproductive effects of resveratrol in *Drosophila melanogaster*. *Toxicol. Res. (Camb.),* **2022**, *11*(1), 101-107. http://dx.doi.org/10.1093/toxres/tfab123 PMID: 35237415

[25] Kozomara, A.; Birgaoanu, M.; Griffiths-Jones, S. miRBase: from microRNA sequences to function. *Nucleic Acids Res.,* **2019**, *47*(D1), D155-D162. http://dx.doi.org/10.1093/nar/gky1141 PMID: 30423142

[26] Sarzynska, J.; Popenda, M.; Antczak, M.; Szachniuk, M. RNA tertiary structure prediction using RNACOMPOSER in CASP15. *Proteins,* **2023**, *91*(12), 1790-1799. http://dx.doi.org/10.1002/prot.26578 PMID: 37615316

[27] Trott, O.; Olson, A.J. AutoDock Vina: Improving the speed and accuracy of docking with a new scoring function, efficient optimization, and multithreading. *J. Comput. Chem.,* **2010**, *31*(2), 455-461. http://dx.doi.org/10.1002/jcc.21334 PMID: 19499576

[28] Mooers, B.H.M. Shortcuts for faster image creation in PyMOL. *Protein Sci.,* **2020**, *29*(1), 268-276. http://dx.doi.org/10.1002/pro.3781

[29] Bitencourt-Ferreira, G.; de Azevedo, W.F., Jr Docking with swissdock. *Methods Mol. Biol.,* **2019**, *2053*, 189-202. http://dx.doi.org/10.1007/978-1-4939-9752-7_12 PMID: 31452106

[30] Murail, S.; de Vries, S.J.; Rey, J.; Moroy, G.; Tufféry, P. SeamDock: An interactive and collaborative online docking resource to assist small compound molecular docking. *Front. Mol. Biosci.,* **2021**, *8*, 716466. http://dx.doi.org/10.3389/fmolb.2021.716466 PMID: 34604303

[31] Daina, A.; Michielin, O.; Zoete, V. SwissADME: A free web tool to evaluate pharmacokinetics, drug-likeness and medicinal chemistry friendliness of small molecules. *Sci. Rep.,* **2017**, *7*(1), 42717. http://dx.doi.org/10.1038/srep42717 PMID: 28256516

[32] Yalçınkaya, S.; Yalçın Azarkan, S.; Karahan Çakmakçı, A.G. Determination of the effect of L. plantarum AB6-25, *L. plantarum* MK55 and S. boulardii T8-3C microorganisms on colon, cervix, and breast cancer cell lines: Molecular docking, and molecular dynamics study. *J. Mol. Struct.,* **2022**, *1261*, 132939. http://dx.doi.org/10.1016/j.molstruc.2022.132939

[33] Bekker, H.; Berendsen, H.J.C.; Dijkstra, E.J.; Achterop, S.; Vondrumen, R.V.; Vanderspoel, D. Gromacs-a parallel computer for molecular-dynamics simulations. In: *4th international conference*

on computational physics; World Scientific Publishing, **1993**; pp. 252-256.

[34] Abraham, M.J.; Murtola, T.; Schulz, R.; Páll, S.; Smith, J.C.; Hess, B.; Lindahl, E. GROMACS: High performance molecular simulations through multi-level parallelism from laptops to supercomputers. *SoftwareX,* **2015**, *1-2*, 19-25. http://dx.doi.org/10.1016/j.softx.2015.06.001

[35] Lindorff-Larsen, K.; Piana, S.; Palmo, K.; Maragakis, P.; Klepeis, J.L.; Dror, R.O.; Shaw, D.E. Improved side-chain torsion potentials for the Amber ff99SB protein force field. *Proteins,* **2010**, *78*(8), 1950-1958. http://dx.doi.org/10.1002/prot.22711 PMID: 20408171

[36] Bjelkmar, P.; Larsson, P.; Cuendet, M.A.; Hess, B.; Lindahl, E. Implementation of the CHARMM force field in GROMACS: analysis of protein stability effects from correction maps, virtual interaction sites, and water models. *J. Chem. Theory Comput.,* **2010**, *6*(2), 459-466. http://dx.doi.org/10.1021/ct900549r PMID: 26617301

[37] Oostenbrink, C.; Villa, A.; Mark, A.E.; Van Gunsteren, W.F. A biomolecular force field based on the free enthalpy of hydration and solvation: The GROMOS force-field parameter sets 53A5 and 53A6. *J. Comput. Chem.,* **2004**, *25*(13), 1656-1676. http://dx.doi.org/10.1002/jcc.20090 PMID: 15264259

[38] Franke, T.F.; Tartof, K.D.; Tsichlis, P.N. The SH2-like Akt homology (AH) domain of c-akt is present in multiple copies in the genome of vertebrate and invertebrate eucaryotes. Cloning and characterization of the *Drosophila melanogaster* c-akt homolog Dakt1. *Oncogene,* **1994**, *9*(1), 141-148. PMID: 8302573

[39] Coudert, E.; Gehant, S.; de Castro, E.; Pozzato, M.; Baratin, D.; Neto, T.; Sigrist, C.J.A.; Redaschi, N.; Bridge, A.; Bridge, A.J.; Aimo, L.; Argoud-Puy, G.; Auchincloss, A.H.; Axelsen, K.B.; Bansal, P.; Baratin, D.; Neto, T.M.B.; Blatter, M-C.; Bolleman, J.T.; Boutet, E.; Breuza, L.; Gil, B.C.; Casals-Casas, C.; Echioukh, K.C.; Coudert, E.; Cuche, B.; de Castro, E.; Estreicher, A.; Famiglietti, M.L.; Feuermann, M.; Gasteiger, E.; Gaudet, P.; Gehant, S.; Gerritsen, V.; Gos, A.; Gruaz, N.; Hulo, C.; Hyka-Nouspikel, N.; Jungo, F.; Kerhornou, A.; Le Mercier, P.; Lieberherr, D.; Masson, P.; Morgat, A.; Muthukrishnan, V.; Paesano, S.; Pedruzzi, I.; Pilbout, S.; Pourcel, L.; Poux, S.; Pozzato, M.; Pruess, M.; Redaschi, N.; Rivoire, C.; Sigrist, C.J.A.; Sonesson, K.; Sundaram, S.; Bateman, A.; Martin, M-J.; Orchard, S.; Magrane, M.; Ahmad, S.; Alpi, E.; Bowler-Barnett, E.H.; Britto, R.; A-Jee, H.B.; Cukura, A.; Denny, P.; Dogan, T.; Ebenezer, T.G.; Fan, J.; Garmiri, P.; da Costa Gonzales, L.J.; Hatton-Ellis, E.; Hussein, A.; Ignatchenko, A.; Insana, G.; Ishtiaq, R.; Joshi, V.; Jyothi, D.; Kandasaamy, S.; Lock, A.; Luciani, A.; Lugaric, M.; Luo, J.; Lussi, Y.; MacDougall, A.; Madeira, F.; Mahmoudy, M.; Mishra, A.; Moulang, K.; Nightingale, A.; Pundir, S.; Qi, G.; Raj, S.; Raposo, P.; Rice, D.L.; Saidi, R.; Santos, R.; Speretta, E.; Stephenson, J.; Totoo, P.; Turner, E.; Tyagi, N.; Vasudev, P.; Warner, K.; Watkins, X.; Zaru, R.; Zellner, H.; Wu, C.H.; Arighi, C.N.; Arminski, L.; Chen, C.; Chen, Y.; Huang, H.; Laiho, K.; McGarvey, P.; Natale, D.A.; Ross, K.; Vinayaka, C.R.; Wang, Q.; Wang, Y. Annotation of biologically relevant ligands in UniProtKB using ChEBI. *Bioinformatics,* **2023**, *39*(1), btac793. http://dx.doi.org/10.1093/bioinformatics/btac793 PMID: 36484697

[40] Lipinski, C.A.; Lombardo, F.; Dominy, B.W.; Feeney, P.J. Experimental and computational approaches to estimate solubility and permeability in drug discovery and development settings 1PII of original article: S0169-409X(96)00423-1. *Adv. Drug Deliv. Rev.,* **2001**, *46*(1-3), 3-26. http://dx.doi.org/10.1016/S0169-409X(00)00129-0 PMID: 11259830

[41] Veber, D.F.; Johnson, S.R.; Cheng, H.Y.; Smith, B.R.; Ward, K.W.; Kopple, K.D. Molecular properties that influence the oral bioavailability of drug candidates. *J. Med. Chem.,* **2002**, *45*(12), 2615-2623. http://dx.doi.org/10.1021/jm020017n PMID: 12036371

[42] Ghose, A.K.; Viswanadhan, V.N.; Wendoloski, J.J. A knowledge-based approach in designing combinatorial or medicinal chemistry libraries for drug discovery. 1. A qualitative and quantitative characterization of known drug databases. *J. Comb. Chem.,* **1999**, *1*(1), 55-68. http://dx.doi.org/10.1021/cc9800071 PMID: 10746014

[43] Wu, M.; Gao, F.; Li, X.; Guo, J.; Wang, T.; Zhang, F. Study on the solubilization effect of 7-ethyl-10-hydroxycamptothecin based on molecular docking and molecular dynamics simulation. *J. Mol. Model.,* **2023**, *29*(2), 58. http://dx.doi.org/10.1007/s00894-023-05455-1 PMID: 36715793

[44] Read, R.D. *Drosophila melanogaster* as a model system for human brain cancers. *Glia,* **2011**, *59*(9), 1364-1376. http://dx.doi.org/10.1002/glia.21148 PMID: 21538561

[45] Weinkove, D.; Neufeld, T.P.; Twardzik, T.; Waterfield, M.D.; Leevers, S.J. Regulation of imaginal disc cell size, cell number and organ size by *Drosophila* class IA phosphoinositide 3-kinase and its adaptor. *Curr. Biol.,* **1999**, *9*(18), 1019-1029. http://dx.doi.org/10.1016/S0960-9822(99)80450-3 PMID: 10508611

[46] Montagne, J.; Stewart, M.J.; Stocker, H.; Hafen, E.; Kozma, S.C.; Thomas, G. *Drosophila* S6 kinase: a regulator of cell size. *Science,* **1999**, *285*(5436), 2126-2129. http://dx.doi.org/10.1126/science.285.5436.2126 PMID: 10497130

[47] Gateff, E.; Schneiderman, H.A. Developmental studies of a new mutant of *Drosophila melanogaster*: Lethal malignant brain tumor (l (2)gl 4). *Am. Zool.,* **1967**, *7*, 760.

[48] Truscott, M.; Islam, A.B.M.M.K.; López-Bigas, N.; Frolov, M.V. *mir-11* limits the proapoptotic function of its host gene, *dE2f1*. *Genes Dev.,* **2011**, *25*(17), 1820-1834. http://dx.doi.org/10.1101/gad.16947411 PMID: 21856777

[49] Xu, P.; Vernooy, S.Y.; Guo, M.; Hay, B.A. The *Drosophila* microRNA Mir-14 suppresses cell death and is required for normal fat metabolism. *Curr. Biol.,* **2003**, *13*(9), 790-795. http://dx.doi.org/10.1016/S0960-9822(03)00250-1 PMID: 12725740

[50] Pinsky, I.; Labeit, S.; Labeit, D.; Ivashchenko, A. Characteristics of miRNA binding sites in mRNAS of human and mouse titin gene. *Int. J. Biol. Chem.,* **2017**, *10*(1), 25-34. http://dx.doi.org/10.26577/2218-7979-2017-10-1-25-34

[51] Hsiao, Y.C.; Yeh, M.H.; Chen, Y.J.; Liu, J.F.; Tang, C.H.; Huang, W.C. Lapatinib increases motility of triple-negative breast cancer cells by decreasing miRNA-7 and inducing Raf-1/MAPK-dependent interleukin-6. *Oncotarget,* **2015**, *6*(35), 37965-37978. http://dx.doi.org/10.18632/oncotarget.5700 PMID: 26513016

[52] Kalinowski, F.C.; Brown, R.A.M.; Ganda, C.; Giles, K.M.; Epis, M.R.; Horsham, J.; Leedman, P.J. microRNA-7: A tumor suppressor miRNA with therapeutic potential. *Int. J. Biochem. Cell Biol.,* **2014**, *54*, 312-317. http://dx.doi.org/10.1016/j.biocel.2014.05.040 PMID: 24907395

[53] Morales-Martínez, M.; Vega, M.I. Role of MicroRNA-7 (MiR-7) in cancer physiopathology. *Int. J. Mol. Sci.,* **2022**, *23*(16), 9091. http://dx.doi.org/10.3390/ijms23169091 PMID: 36012357

[54] Correa-Medina, M.; Bravo-Egana, V.; Rosero, S.; Ricordi, C.; Edlund, H.; Diez, J.; Pastori, R.L. MicroRNA miR-7 is preferentially expressed in endocrine cells of the developing and adult human pancreas. *Gene Expr. Patterns,* **2009**, *9*(4), 193-199. http://dx.doi.org/10.1016/j.gep.2008.12.003 PMID: 19135553

[55] Hong, T.; Ding, J.; Li, W. miR-7 reverses breast cancer resistance to chemotherapy by targeting MRP1 and BCL2. *OncoTargets Ther.,* **2019**, *12*, 11097-11105. http://dx.doi.org/10.2147/OTT.S213780 PMID: 31908478

[56] Primavera, E.; Palazzotti, D.; Barreca, M.L.; Astolfi, A. Computer-aided identification of kinase-targeted small molecules for cancer: A review on AKT protein. *Pharmaceuticals (Basel),* **2023**, *16*(7), 993. http://dx.doi.org/10.3390/ph16070993 PMID: 37513905

[57] Rothenberg, M.L. Irinotecan (CPT-11): Recent developments and future directions--colorectal cancer and beyond. *Oncologist,* **2001**, *6*(1), 66-80. http://dx.doi.org/10.1634/theoncologist.6-1-66 PMID: 11161230

[58] Mirzoyan, Z.; Sollazzo, M.; Allocca, M.; Valenza, A.M.; Grifoni, D.; Bellosta, P. *Drosophila melanogaster*: A model organism to study cancer. *Front. Genet.,* **2019**, *10*, 51. http://dx.doi.org/10.3389/fgene.2019.00051 PMID: 30881374